

Supporting Information for

Catalytic reduction of oxygen to water by non-heme iron complexes: exploring the effect of the secondary coordination sphere proton exchanging site

Aakash Santra,^a Avijit Das,^a Simarjeet Kaur,^a Priya Jain,^a Pravin P. Ingole,^a Sayantan Paria^{a*}

^aDepartment of Chemistry, Indian Institute of Technology Delhi, Hauz Khas, New Delhi 110016; Email: sparia@chemistry.iitd.ac.in

General Consideration. All solvents and chemicals used in this study were purchased commercially and used as it is. Acetonitrile, methanol, and diethyl ether were purified following standard procedures. Air-sensitive compounds were prepared using standard Schlenk techniques or in a N₂-filled glove box. **Caution:** *Although no problems were encountered during the synthesis of the complexes, perchlorate salts are potentially explosive and should be handled with care!*¹

NMR data of the ligands and Fe complexes were collected using a Bruker 400 and 500 MHz NMR spectrometer at 25 °C. X-band EPR data of the Fe^{III} complexes were recorded in a Bruker A300 spectrometer at 77 K using a liquid nitrogen finger dewar. ESI-mass data of the ligand and Fe complex was measured in a Waters Xevo-G2XQTOF instrument. IR data were obtained on KBr palettes using a Nicolet protégé 460 ESP instrument. CHN analysis of all Fe complexes were performed in a PerkinElmer 2400 Series II CHNS/O instrument.

Spectrochemical Measurements. Kinetic studies were performed using an Agilent 8454 diode-array or Cary 60 UV-vis spectrophotometer equipped with a UNISOKU cryostat for controlling the temperature. The catalytic ORR experiments were performed in a 1-cm pathlength cuvette placed in the UV-vis spectrophotometer, containing an acetonitrile solution of 0.02 mM complex (catalytic amount), 1 mM of decamethylferrocene (Fc*), 20 mM trifluoroacetic acid (TFAH), and oxygen (saturated). The progress of the reaction was monitored through the formation of decamethylferrocenium cation (Fc^{*+}) at 780 nm in the UV-vis spectrum. The pseudo-first-order rate constant (k_{obs}) values were obtained from the slope of a plot of $\ln(A_{\infty}-A)$ vs. time (s). The second-order rate constants were obtained from the slope of a plot of k_{obs} vs. [substrate]. To establish the dependence of substrate concentration towards catalytic ORR, a plot of k_{obs} vs. [substrate] was determined at different concentrations of the substrate. For every experiment, the concentration of one substrate was varied (e.g., complex); however, the other substrate concentrations (Fc*, TFAH, and O₂) were kept constant. Acetonitrile solution of different oxygen concentrations was prepared by mixing the required volume of an O₂ saturated acetonitrile solution with a deoxygenated acetonitrile solution. The third-order rate constant (k_{cat} , M⁻² s⁻¹) value of **1** for ORR reaction was determined using eq S1 and the slope of Figure 8B.

$$k_{\text{cat}} (\text{ORR}) = \frac{(\text{slope of the plot of } k_{\text{obs}} (\text{M}^{-1} \text{s}^{-1}) \text{ vs. } [\text{complex}])}{[\text{TFAH}]} \quad (\text{S1})$$

For the reactions following zero-order kinetics (H₂O₂RR of **1** and ORR of **3**), the initial rate of the reactions (k_i , M s⁻¹) was determined from the slope of a plot of [Fc^{*+}] formation vs. reaction time (s). The substrate dependence of such reactions was determined from the plots of k_i vs. [substrate]. The second-order rate constant (k_{cat} , M⁻¹s⁻¹) for the H₂O₂RR of **1** was determined using eq S2 and the slope of the plot of Figure S65, SI.

$$k_{\text{cat}} (\text{H}_2\text{O}_2\text{RR}) = \frac{(\text{slope of the plot of initial rate } (k_i, \text{ M/s}) \text{ vs. } [\text{complex}])}{[1]} \quad (\text{S2})$$

Likewise, we determined the k_{cat} (M⁻¹s⁻¹) of ORR of **3** using eq S3 and the slope of the plot described in Figure 10A.

$$k_{\text{cat}} (\text{ORR}) = \frac{(\text{slope of the plot of initial rate } (k_i, \text{ M/s}) \text{ vs. } [\text{complex}])}{[\text{complex}]} \quad (\text{S3})$$

The chemical turnover frequency (TOF) of the ORR of **3** (Figure S58D) and H₂O₂RR of **1** (Figure S64D) was determined using eq S4.

$$\text{TOF} = \frac{(\text{initial rate of ORR or H}_2\text{O}_2\text{RR})/n}{[\text{complex}]} \quad (\text{S4})$$

For the ORR reaction, n = 4 and H₂O₂RR, n = 2 was used for the calculation of chemical TOF.

Activation Parameters. Further, the k_{cat} value of ORR was determined chemically at different temperatures to estimate the activation parameters using eq S5. $\ln(k_{\text{cat}}/T)$ was plotted against $1/T$ at different temperatures. ΔH^\ddagger and ΔS^\ddagger values were estimated from the slope and intercept of the plot of $\ln(k_{\text{cat}}/T)$ vs. $1/T$, (eq S5), respectively.

$$\ln\left(\frac{k_{\text{cat}}}{T}\right) = -\frac{\Delta H^\ddagger}{R} \cdot \frac{1}{T} + \ln\frac{k_B}{h} + \frac{\Delta S^\ddagger}{R} \quad (\text{S5})$$

Here, ΔH^\ddagger is activation enthalpy, ΔS^\ddagger is activation entropy, T is temperature, h is Planck's constant, k_B is Boltzmann's constant, and R is Universal gas constant.

Electrochemical Measurements. Cyclic voltammetry (CV) and differential pulse voltammetry (DPV) of the Fe complexes were measured in acetonitrile containing a large excess (100 times with respect to the catalyst conc.) of ⁿBu₄NPF₆ as the supporting electrolyte, using a CH760E potentiostat (CH Instruments, USA) in a conventional three-electrode set-up. Glassy carbon (ID: 3 mm) working electrode, Pt wire counter electrode, and Ag/AgCl in saturated KCl as the reference electrode were utilized during the measurements. After the measurement of CV data of the Fe complexes, the Fe^{III}/Fe^{II} potential of ferrocene in acetonitrile containing ⁿBu₄NPF₆ as the supporting electrolyte was measured. Then, the potential window was standardized with respect to the Fc⁺/Fc couple, and the potential values were reported with respect to the Fc⁺/Fc couple.

CV/DPV of the Fe^{II} complexes were measured in an N₂-filled glove box. ORR of **1** (0.5 mM) was investigated in an oxygen-saturated acetonitrile solution containing 20 equiv. of TFAH.

Diffusion Coefficient Calculations for Redox Peak

The Diffusion coefficients (D) have been determined from the redox peaks using the Randles-Ševčík equation (eq S6):

$$i_{\text{redox}} = 0.446 n^{3/2} A C_{\text{Cat}} (vF^3 D_{\text{Obs}}/RT)^{1/2} \quad (\text{S6})$$

Where, D_{obs} = Diffusion Coefficient, i_{redox} = Reduction peak current of the redox couple under N₂. n=1 is the number of electrons transferred in the redox process. C = concentration of

catalyst, $F = 96485$ C/mol, Faraday constant. A = surface area of glassy carbon working electrode. $T = 298$ K, $R =$ ideal gas constant (8.314 J/K).

The value of D_{obs} has been calculated for the $\text{Fe}^{\text{III}}/\text{Fe}^{\text{II}}$ redox peak by a variable scan rate using eq S7.

$$\text{Slope} = \left(\frac{i_p}{\sqrt{v}} \right) = k.n^{3/2}.A.\sqrt{D}.C \quad (\text{S7})$$

For Complex 1:

$k = 2.69 \times 10^5$ C mol⁻¹v^{-1/2}, $A = 0.0707$ cm², $n = 1$, $C = 5 \times 10^{-7}$ mol cm⁻³, Slope = 9.34×10^{-6} A V^{-1/2} s^{1/2}, $D_{\text{obs}} = 9.64 \times 10^{-7}$ cm² s⁻¹

For Complex 2:

$k = 2.69 \times 10^5$ C mol⁻¹v^{-1/2}, $A = 0.0707$ cm², $n = 1$, $C = 5 \times 10^{-7}$ mol cm⁻³, Slope = 7.93×10^{-6} A V^{-1/2} s^{1/2}, $D_{\text{obs}} = 6.95 \times 10^{-7}$ cm² s⁻¹

Calculation Overpotential for ORR in acetonitrile

We have calculated the effective overpotential of ORR following the literature procedure and reported pK_a and $\log(K_{\text{HAH}})$ value of TFAH in acetonitrile (eq S8).²⁻⁴

$$E_{O_2/H_2O}^{\circ} = 1.21 - 0.0592(pK_a) + \frac{2.303 RT}{4F} \log(4K_{\text{AHA}}) \quad (V \text{ vs } Fc^+/Fc) \quad (\text{S8})$$

After putting all values, $pK_a = 12.65$, $R = 8.314$ J/K, $T = 298$ K, $F = 96485$ C/mol, $\log(K_{\text{AHA}}) = 3.9$. Where K_{AHA} = homoconjugation equilibrium constant for TFA in MeCN, we obtain

$$E_{O_2/H_2O}^{\circ} = 0.53 \text{ V vs } Fc^+/Fc$$

$$\eta = E_{O_2/H_2O}^{\circ} - \frac{E_{\text{Cat}}}{2}$$

For Complex 1:

$E_{\text{cat}/2} = -0.45$ V (0.1 V/s)

Calculated Overpotential,

$\eta_{O_2/H_2O} = 0.53 - (-0.45) = 0.98$ V (vs Fc^+/Fc)

Electrochemical Kinetics.

To find out the scan-rate independent region, CV data of **1** (0.5 mM) were collected at multiple scan rates in the presence of TFAH (10 mM) and 50 mM ⁿBu₄NPF₆ in oxygen-saturated acetonitrile solution at 25 °C. It was observed that a minimum scan rate of 6 V/s was necessary to achieve i_{cat} independence region. Thus, the measurement of different substrate-dependent experiments was performed at a scan rate of 6 V/s.

For the substrate dependence study, CV data of **1** (0.5 mM) were measured at different concentrations of TFAH (1.25-7.5 mM) in oxygen-saturated acetonitrile containing 50 mM ⁿBu₄NPF₆ as the supporting electrolyte at 6 V/s scan rate. Likewise, we varied the complex concentration at a constant TFAH concentration (10 mM) in an oxygen-saturated acetonitrile solution. The plots of $\log(J, \text{A/cm}^2)$ vs. $\log([\text{TFAH}])$ (Fig. 6C) and $\log(J, \text{A/cm}^2)$ vs. $\log([\mathbf{1}])$ (Fig. S38) follow a linear relationship, indicating first-order dependence (i.e. $m = 1$) of both

TFAH and complex **1**, according to eq S9.⁵ Likewise, we obtain a first-order dependence of O₂ concentration.

$$i_{cat} = n_{cat}FA[cat](Dk_{cat}[Q]^m)^{1/2} \quad (S9)$$

Thus, kinetic studies establish the rate eq S10-S11 (eq 2-3 in text) for the electrocatalytic ORR of **1**.

$$\text{rate} = k_{obs} [\mathbf{1}] \quad (S10)$$

$$k_{obs} = k_{cat} [\text{TFAH}]^1 [\text{O}_2]^1 \quad (S11)$$

The k_{obs} values of different TFAH variation experiments were obtained using eq S12 (eq 1 in main text).

$$\frac{i_{cat}}{i_p} = \frac{n_{cat}}{0.4463n_p^{3/2}} \sqrt{\frac{RTk_{obs}}{Fv}} \quad (S12)$$

A plot of k_{obs} vs. [TFAH] follows a linear relationship, and k_{H^+} value was obtained from the slope of the plot (Fig. 6D, main text). An apparent third-order rate constant (k_{cat}) (first order with respect to [cat], first order with respect to [TFAH], and first order with respect to [O₂]) has been calculated using eq S13.

$$k_{cat} = k_{H^+}/[\text{O}_2] \quad (S13)$$

$$k_{cat} = 2.7 \times 10^7 \text{ M}^{-2} \text{ s}^{-1}$$

TOF Calculation. CV data of **1** (0.5 mM) in O₂ saturated (6.0 mM) acetonitrile containing 50 mM ⁿBu₄NPF₆ in the presence of 10 mM TFAH at different scan rates were taken. A saturation of catalytic current has been observed at a scan rate (ν) of 6 V s⁻¹. Then, the TOF has been determined using eq. S12.^{6,7}

Rotating Ring Disk Electrode (RRDE) instrument:

Hydrodynamic voltammetry experiment. The hydrodynamic voltammetric experiments were performed in a Metrohm autolab 204N bipotentiostat using a four-electrode (RRDE) cell setup. A Metrohm RRDE assembly has been used as a working electrode (W.E.) consisting of a glassy carbon disk (diameter - 5 mm) as W.E.-1 and a thin concentric Pt ring (S = 0.1 cm²) as W.E. 2. A Pt wire as counter electrode and Ag/AgCl in saturated KCl as the reference electrode was used during the measurements.

The LSV polarisation curves were recorded with Complex **1** (0.5 mM) in acetonitrile in the presence of 0.5 M ⁿBu₄NPF₆ under an O₂ atmosphere at 200 rpm rotation rate, while a constant potential of 1.23 V vs Ag/AgCl was applied on the Pt ring.

The % yield of H₂O₂ and calculation of the number of electrons (n) involved in the ORR was obtained according to eq S14, and eq S15.

$$\% \text{H}_2\text{O}_2 = \frac{2 \times \left(\frac{i_{ring}}{N} \right)}{i_{disk} + \left(\frac{i_{ring}}{N} \right)} \times 100 \quad (S14)$$

$$n = \frac{4 \times i_{disk}}{i_{disk} + \left(\frac{i_{ring}}{N}\right)} \quad (S15)$$

Where i_{ring} and i_{disk} are the values of ring and disk current, respectively, at a potential E. N is the collection efficiency of the electrode. We have calculated a collection efficiency (CE) of 0.249.

% H₂O₂ Calculated~ 0.52.

Calculated n~ 4.0.

It's important to note here that

H₂O₂ Selectivity Check. The ORR reaction was monitored by UV-vis spectroscopy. Once the time trace at 780 nm was saturated, 100 μL of the reaction solution was taken and immediately diluted with 5 mL of distilled water and 10 mL of DCM. Then, 3 mL of the water-based solution was taken in a cuvette, and 100 μL of a 0.1 M solution of Ti(O)SO₄ was added to it. The reaction was then monitored at 405 nm in UV-vis spectroscopy. No change of absorbance was obtained at 405 nm with the reaction solution. However, the addition of H₂O₂ to the reaction mixture resulted in the immediate generation of the peak at 405 nm.

Kinetic Isotope Effect. The kinetic isotope effect (KIE) has been examined in the presence of trifluoroacetic acid-*d* (TFAD). The k_2 value for the ORR has been calculated from the concentration variation (TFAH and TFAD) experiments, and the KIE was determined from the ratio of k_2^H/k_2^D .

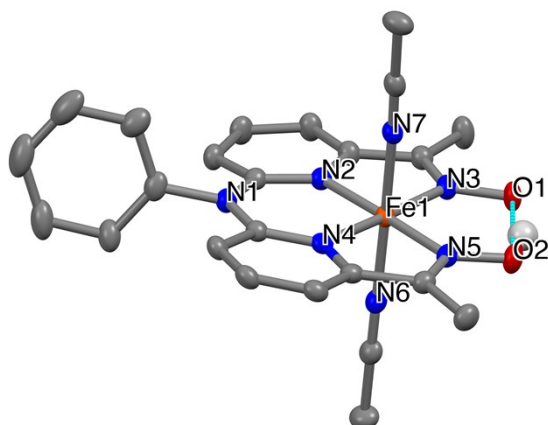
X-ray Crystallography. Single crystals of Fe^{II} Complexes (**1a**, **2a**, and **3a**), suitable for X-ray diffraction, were obtained by diffusing diethyl ether into the complex solution in acetonitrile. Crystal data was measured on a Bruker D8 VENTURE Microfocus diffractometer system equipped with a PHOTON II Detector, with Mo K_α radiation ($\lambda = 0.71073 \text{ \AA}$) and controlled by the APEX4 (v2022.1-1) software package. The raw data were integrated and corrected for Lorentz and polarization effects with the aid of the Bruker APEX4 program suite. Absorption corrections were performed by using SADABS. Structures were solved by the intrinsic phasing method and refined against all data in the reported 2θ ranges by the full-matrix least squares method based on F² using the SHELXL program suite⁸ with all observed reflections. Hydrogen atoms at idealized positions were included in the final refinements. The non-hydrogen atoms were treated anisotropically. Diagrams for the complexes were prepared using Mercury software.⁹ Crystallographic data of Fe complexes are given in Table S1, and bond parameters are mentioned in Table S2. CCDC numbers 2290392, 2290393 and 2314421 contain crystallographic data of the Fe complex.

Table S1. Crystallographic parameters of the complex **1a**, **2a** and **3a**.

Identification Code	[Fe ^{II} (HL)]BPh ₄ (1a)	[Fe ^{II} (Me ₂ L)(ClO ₄) ₂] (2a)	[Fe ^{II} (BPh ₂ L)]BPh ₄ (3a)
Empirical formula	C ₂₀₈ H ₂₁₆ N ₂₈ O ₁₂ B ₄ Fe ₄	C _{3.33} H _{3.89} Cl _{0.22} Fe _{0.11} NO _{1.11}	C _{4.33} H _{4.33} B _{0.13} Fe _{0.07} N _{0.52} O _{0.2}
Formula weight	3566.72	89.82	71.922
Temperature/K	100.00	100(2)	116.00

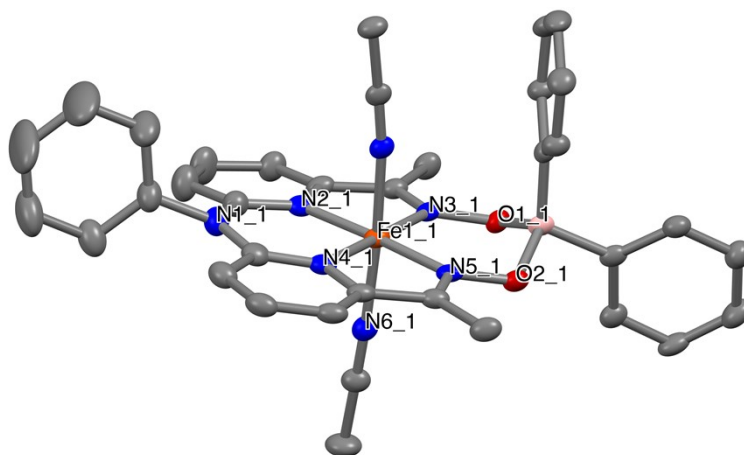
Crystal system	tetragonal	triclinic	monoclinic
Space group	I-4	P-1	P2 ₁ /c
a/Å	26.5624(9)	8.1243(3)	18.5453(11)
b/Å	26.5624(9)	13.3350(4)	15.6403(8)
c/Å	14.7302(7)	17.7851(5)	21.1386(11)
α /°	90	102.0800(10)	90
β /°	90	90.3000(10)	109.232(2)
γ /°	90	96.5610(10)	90
Volume/Å ³	10393.1(9)	1870.95(10)	5789.2(6)
Z	2	18	61
ρ calc/g/cm ³	1.140	1.435	1.258
μ /mm ⁻¹	0.336	0.611	0.315
F(000)	3760.0	836.0	2314.8
Radiation	MoK α (λ = 0.71073)	MoK α (λ = 0.71073)	Mo K α (λ = 0.71073)
2 Θ range for data collection/°	5.368 to 56.606	4.302 to 50.066	3.5 to 50.16
Index ranges	-35 \leq h \leq 35, -35 \leq k \leq 35, -19 \leq l \leq 19	-9 \leq h \leq 9, -15 \leq k \leq 15, -21 \leq l \leq 21	-22 \leq h \leq 22, -18 \leq k \leq 18, -25 \leq l \leq 25
Reflections collected	255937	74918	153314
Independent reflections	12838 [R_{int} = 0.1139, R_{sigma} = 0.0300]	6602 [R_{int} = 0.0462, R_{sigma} = 0.0227]	10215 [R_{int} = 0.1461, R_{sigma} = 0.0620]
Data/restraints/parameters	12838/1/585	6602/0/477	10215/0/682
Goodness-of-fit on F ²	1.038	1.050	1.058
Final R indexes [$I \geq 2\sigma(I)$]	R_1 = 0.0299, wR_2 = 0.0763	R_1 = 0.0590, wR_2 = 0.1568	R_1 = 0.0524, wR_2 = 0.1270
Final R indexes [all data]	R_1 = 0.0316, wR_2 = 0.0773	R_1 = 0.0604, wR_2 = 0.1581	R_1 = 0.0734, wR_2 = 0.1418
Largest diff. peak/hole / e Å ⁻³	0.25/-0.20	2.12/-1.39	0.55/-0.54

Table S2. Selected bond length (Å) and bond angles (°) observed in the X-ray structure of **1a**.



Bonds distance (Å) or angles (°)	1a
Fe1–N2	1.9019 (16)
Fe1–N3	1.9041 (18)
Fe1–N4	1.9107 (17)
Fe1–N5	1.8924 (16)
Fe1–N6	1.9350(17)
Fe1–N7	1.9275(16)
N2–Fe1–N4	95.47(7)
N3–Fe1–N2	83.31(7)
N5–Fe1–N3	97.78(7)
N4–Fe1–N5	83.45(7)
N6–Fe1–N2	89.93(7)
N6–Fe1–N3	90.44(7)
N6–Fe1–N4	90.37(7)
N6–Fe1–N5	88.98(7)
N7–Fe1–N2	90.20(7)
N7–Fe1–N3	91.02(7)
N7–Fe1–N4	88.17(7)
N7–Fe1–N5	90.86(7)
N7–Fe1–N6	178.53(8)

Table S3. Selected bond length (Å) and bond angles (°) were observed in the X-ray structure of **2a**.



Bonds distance (Å) or angles (°)	3a
Fe1–N2	1.906(2)
Fe1–N3	1.882(2)
Fe1–N4	1.901(2)
Fe1–N5	1.882(2)
Fe1–N6	1.950(2)
Fe1–N7	1.932(2)
N3–O1	1.365(3)
N5–O2	1.371(3)
B1–O1	1.539(3)
B1–O2	1.524(3)
N2–Fe1–N4	95.52(10)
N3–Fe1–N2	83.40(10)
N5–Fe1–N3	97.92(10)
N4–Fe1–N5	83.14(10)
N6–Fe1–N2	88.61(10)
N6–Fe1–N3	88.40(9)
N6–Fe1–N4	91.14(9)
N6–Fe1–N5	89.38(9)
N7–Fe1–N2	88.28(9)
N7–Fe1–N3	93.48(9)
N7–Fe1–N4	86.93(9)
N7–Fe1–N5	93.68(9)
N7–Fe1–N6	176.16(10)
Fe1–N3–O1	125.52(16)
Fe1–N5–O2	124.11(16)
N3–O1–B1	116.60(19)
N5–O2–B1	115.70(19)
O1–B1–O2	112.7(2)

Experimental Section

Synthesis. 1,1'-((phenylazanediy)bis(pyridine-6,2-diyl))bis(ethan-1-one) dioxime (H₂L), and the [Zn(H₂L)(Cl)]Cl complexes were prepared according to the reported literature procedure.¹⁰

Me₂L. 1,1'-((phenylazanediy)bis(pyridine-6,2-diyl))bis(ethan-1-one) (0.2 g, 0.6 mmol) was dissolved in 20 mL of ethanol, and then, sodium acetate (0.39 g, 4.8 mmol) and methoxylamine hydrochloride (0.2 g, 2.4 mmol) were added to it under stirring condition. The reaction solution refluxed at *ca.* 90 °C for 5h. The reaction solution was then cooled down, and the solvent was removed under reduced pressure. The resulting crude product was redissolved in ethyl acetate, washed with brine solution, and dried over anhydrous sodium sulfate. Removal of the solvent resulted in Me₂L. Yield: 80 % (0.19 g). ESI-MS (positive ion mode, CH₃CN): *m/z* (%): 390.1 ([Me₂L + H]⁺), 391.1 ([Me₂L + 2H]⁺). ¹H NMR (500 MHz, DMSO-*d*₆, 25 °C): δ 2.04 (s, 6H), 4.02 (s, 6H), 7.02-7.04 (d, 2H), 7.24-7.28 (d, 2H), 7.38-7.41 (t, 2H), 7.52-7.53 (d, 2H), 7.55 (s, 3H). Elemental analysis calcd (%) for Me₂L (C₂₂H₂₃N₅O₂, 389.45 g/mol): C, 67.85, H, 5.95, N, 17.98. Found: C, 67.75, H, 5.99, N, 17.88.

[Fe^{III}(HL)(CH₃CN)₂](ClO₄)₂ (1). A methanolic solution of Fe^{III}(ClO₄)₃.xH₂O (0.05 g, 0.13 mmol) was added dropwise to a methanol solution of H₂L (0.05 g, 0.13 mmol). The reaction solution immediately became dark brown, which was allowed to stir for 30 min at room temperature and then filtered using a glass crucible. The solvent was removed under reduced pressure, and the blackish residue was re-dissolved in a minimum volume of acetonitrile. Excess diethyl ether was added to the acetonitrile solution under stirring conditions, which resulted in the formation of a dark brown precipitate, which was filtered and isolated. Yield 72 % (0.07 g). ESI-MS (positive ion mode, CH₃CN): *m/z* 416.08 ([Fe(HL)]⁺). IR (cm⁻¹): 3433 (br), 1629 (m), 1443 (m), 1371(m), 1267 (m), 1146 (m), 1111 (s), 1088 (s), 791 (m), 628 (s). UV-vis (λ, nm in CH₃CN): 468, 323, and 264. Elemental analysis calcd (%) for C₂₀H₁₈Cl₂FeN₅O₁₄·CH₃CN): C, 40.27, H, 3.23, N, 12.81. Found: C, 40.52, H, 3.35, N, 12.78.

[Fe^{II}(HL)(CH₃CN)₂](BPh₄) (1a). The ligand H₂L (0.05 g, 0.13 mmol) and Fe^{II}(ClO₄)₂.xH₂O (0.03 g, 0.13 mmol) were dissolved in acetonitrile and mixed together under an N₂ environment inside the glove box. The solution became reddish in color and was allowed to stir at room temperature for a few minutes. After that, one equiv. NaBPh₄ (0.05 g, 0.13 mmol) was dissolved in acetonitrile and added to the reaction mixture. The solution immediately became orange, which was allowed to stir for 30 min inside the glove box and then filtered using a glass crucible. Further, the volume of the filtrate was minimized under reduced pressure, and excess diethyl ether was added to the acetonitrile solution, which resulted in the formation of an orangish precipitate, which was filtered and isolated. Single crystals suitable for X-ray diffraction were obtained by diffusing diethyl ether into an acetonitrile solution of the complex at -10 °C. Yield: 0.07 g (60 %). ESI-MS (positive ion mode, CH₃CN), *m/z*: 416.08 [Fe(HL)]⁺, 417.08 [Fe(HL) + H]⁺. IR (cm⁻¹): 3444 (br), 3052 (m), 1583(m), 1438 (s), 1363 (s), 1266 (m), 1173 (m), 1115 (s), 1088 (s), 785 (m), 734 (s), 705 (s), 610 (m), 519 (w). UV-vis (λ, nm in CH₃CN): 481, 359, and 337. Elemental analysis calcd (%) for 1a (C₄₄H₃₈BF₄FeN₅O₂·2CH₃CN): C, 70.52; H, 5.42; N, 11.99; Found: C, 70.22; H, 5.32, N, 11.79.

[Fe^{III}(Me₂L)(CH₃CN)₂](ClO₄)₃ (2**).**

A methanolic solution of Fe^{III}(ClO₄)₃.xH₂O (0.03 g, 0.07 mmol) was added dropwise to a stirring solution of Me₂L (0.03 g, 0.07 mmol) in 3 mL of methanol. The reaction solution immediately became orange, which was allowed to stir for 30 min at room temperature and then filtered using a glass crucible. Then, methanol was removed under reduced pressure, and the resultant residue was re-dissolved in a minimum volume of acetonitrile. Excess diethyl ether was added to the acetonitrile solution under stirring conditions, which resulted in the formation of a brown precipitate. The precipitated Fe complex was filtered, isolated, and dried under a vacuum. Yield 79 % (0.05 g). IR (cm⁻¹): 3431 (br), 2931 (w), 1613 (m), 1571(m), 1449 (m), 1299 (w), 1141 (s), 1116 (s), 1089 (s), 1051 (s), 798 (m), 700 (w), 630 (m). UV-vis (λ, nm, in CH₃CN): 269, 305, 357, and 488. Elemental analysis calcd (%) for **2** (C₂₂H₂₃Cl₃FeN₅O₁₀): C, 35.53, H, 3.12, N, 9.42. Found: C, 35.93, H, 3.30, N, 10.05.

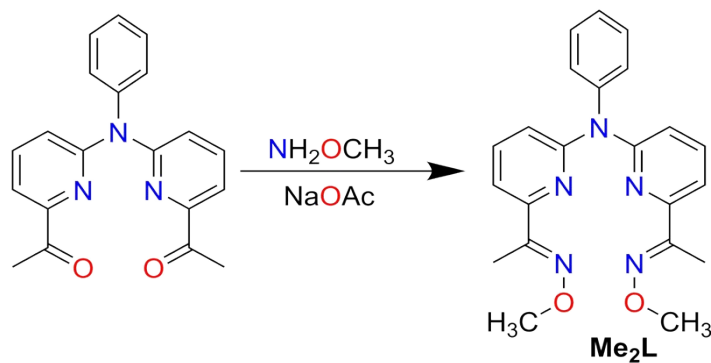
[Fe^{II}(Me₂L)(CH₃CN)₂](ClO₄)₂ (2a**).**

The ligand Me₂L (0.05 g, 0.12 mmol) and Fe^{II}(ClO₄)₂.xH₂O (0.03 g, 0.12 mmol) were dissolved in acetonitrile and mixed together under an N₂ environment inside the glove box. The solution became reddish in color and was allowed to stir at room temperature for a few minutes and then filtered using a glass crucible. Then, the volume of the solvent was minimized under reduced pressure, and excess diethyl ether was added to the acetonitrile solution, which resulted in the formation of an orangish precipitate, which was filtered and isolated. Single crystals suitable for X-ray diffraction, were obtained by diffusing diethyl ether into an acetonitrile solution of the complex at -10 °C. Yield: 0.07 g (77 %). IR (cm⁻¹): 3431 (br), 2936 (w), 1575 (m), 1447 (m), 1369 (m), 1299 (m), 1144 (s), 1116 (s), 1088 (s), 1052 (s), 894 (w), 796 (m), 705 (w), 629 (m). UV-vis (λ, nm in CH₃CN): 331, 358, and 486. Elemental analysis calcd (%) for **2a** (C₂₂H₂₃Cl₂FeN₅O₁₀·CH₃CN): C, 42.07, H, 3.82, N, 12.26. Found: C, 42.23, H, 4.02, N, 12.53.

[Fe^{II}(BPh₂L)(CH₃CN)₂](BPh₄) (3a**).** An acetonitrile solution of Fe^{III}(ClO₄)₂.xH₂O (0.05 g, 0.13 mmol) was added dropwise to an acetonitrile solution of ligand H₂L (0.05 g, 0.13 mmol) inside a N₂ filled globe box. The solution became reddish in color, and was allowed to stir at room temperature for a few minutes. After that, an acetonitrile solution of an excess of NaBPh₄ (0.12 g, 0.34 mmol) was added dropwise to the reaction solution, which resulted in an immediate color change of the solution from red to orange. The resulting solution was allowed to stir for 30 min and then filtered using a glass crucible. The volume of the solvent was then reduced under vacuum, and excess diethyl ether was added to the acetonitrile solution, which resulted in the formation of an orangish precipitate, which was filtered and isolated. Single crystals, suitable for X-ray diffraction were obtained by diffusing diethyl ether into an acetonitrile solution of the complex at -10 °C. Yield: 0.11 g (81 %). ESI-MS (positive ion mode, CH₃CN), *m/z*: 580.16 [BPh₂L + Fe]⁺, 581.16 [BPh₂L + Fe + H]⁺. IR (cm⁻¹): 3440 (br), 2924 (s), 1438 (s), 1360 (s), 1149 (s), 1111 (s), 1079 (s), 737 (m), 703 (s). UV-vis (λ, nm): 484, 405, 360, 337. Elemental analysis calcd (%) for **3a**. (C₅₆H₄₇B₂FeN₅O₂·2CH₃CN·H₂O): C, 72.09; H, 5.55; N, 9.81; Found: C, 72.51; H, 5.61, N, 9.75.

3a can also be synthesized by adding NaBPh₄ to the isolated Fe^{III} complex **1** in acetonitrile at room temperature.

In-situ generation of 3. One equiv. of CAN was added to a methanolic or tetrahydrofuran solution of **3a** at 25 °C, and the UV-vis or EPR spectrum of the resulting solution was measured. Likewise, during the kinetic studies, **3** was generated in acetonitrile by adding one equiv. of CAN to **3a** in acetonitrile.



Scheme S1. Synthesis of Me₂L.

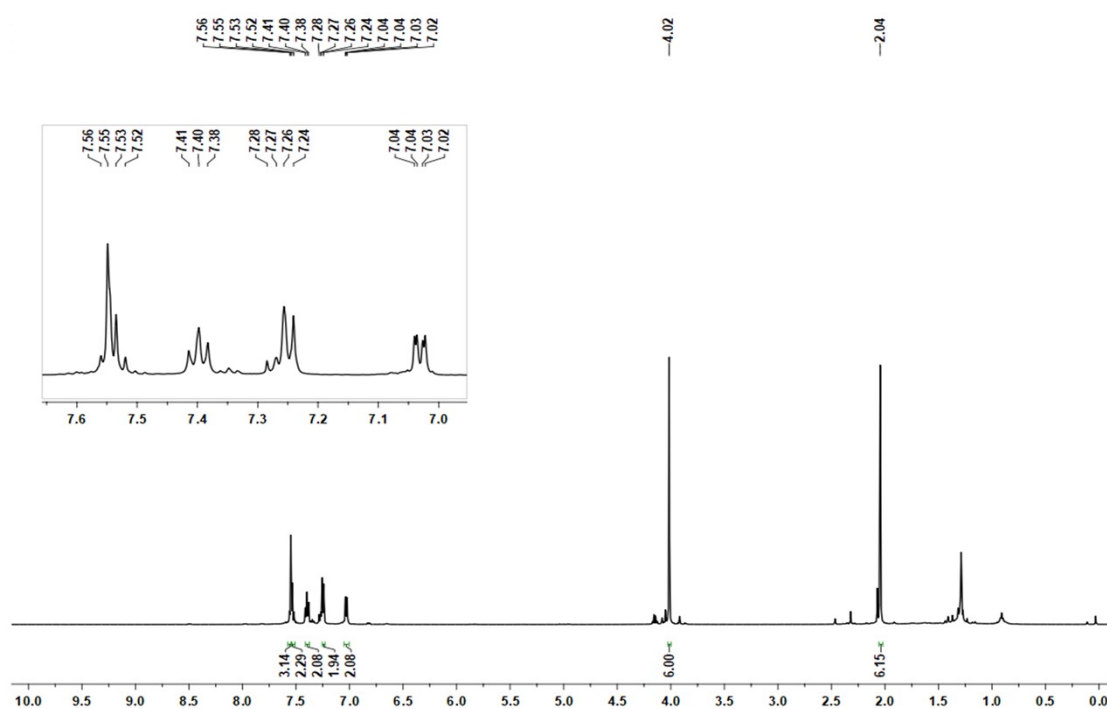


Figure S1. ¹H NMR of Me₂L in DMSO-*d*₆ (500 MHz) at 25 °C.

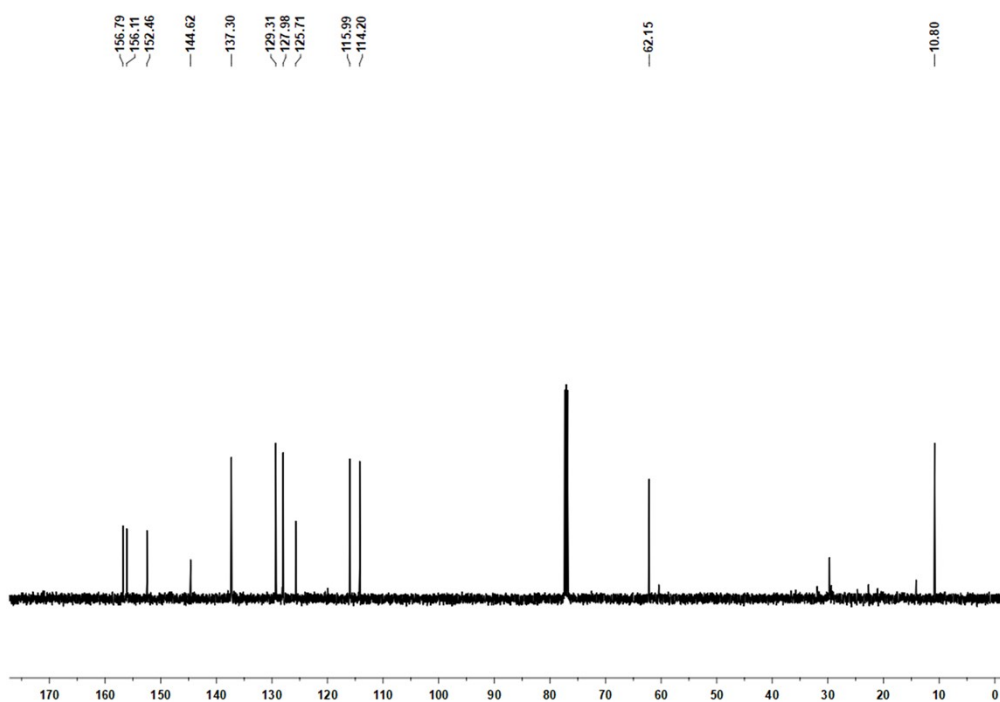


Figure S2. ^{13}C NMR of Me_2L in $\text{DMSO-}d_6$ (500 MHz) at 25 °C.

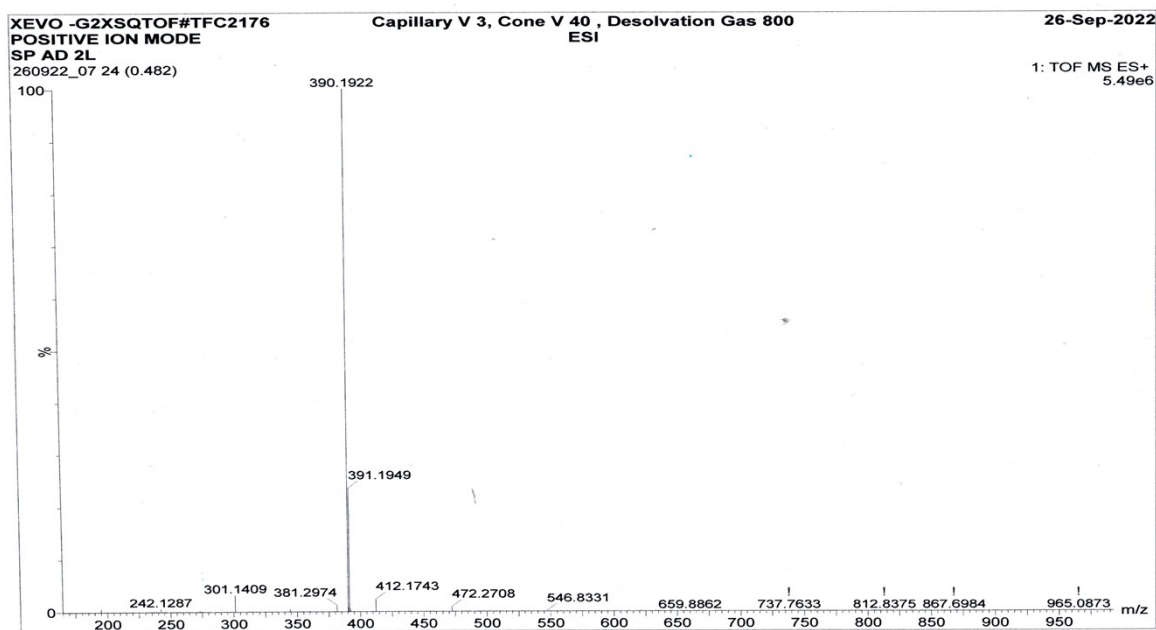


Figure S3. The ESI-mass spectrum of Me_2L in methanol (positive ion mode).

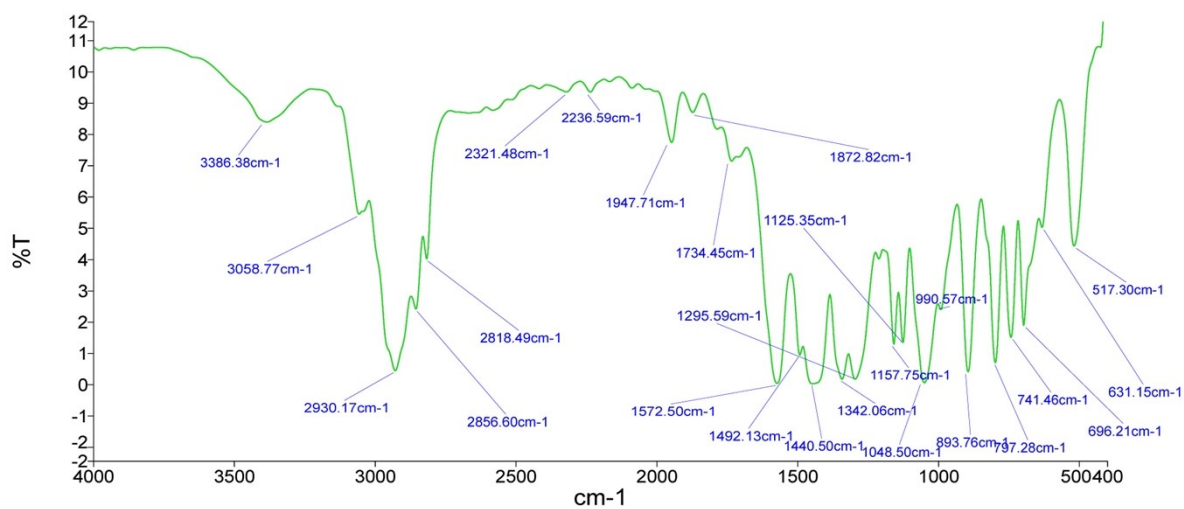


Figure S4. FT-IR spectrum of Me₂L obtained on KBr pellet.

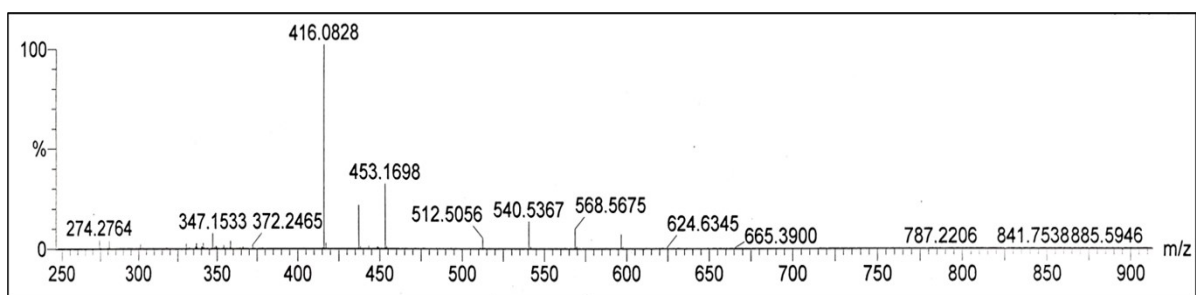


Figure S5. The ESI-mass spectrum of **1** in acetonitrile (positive ion mode).

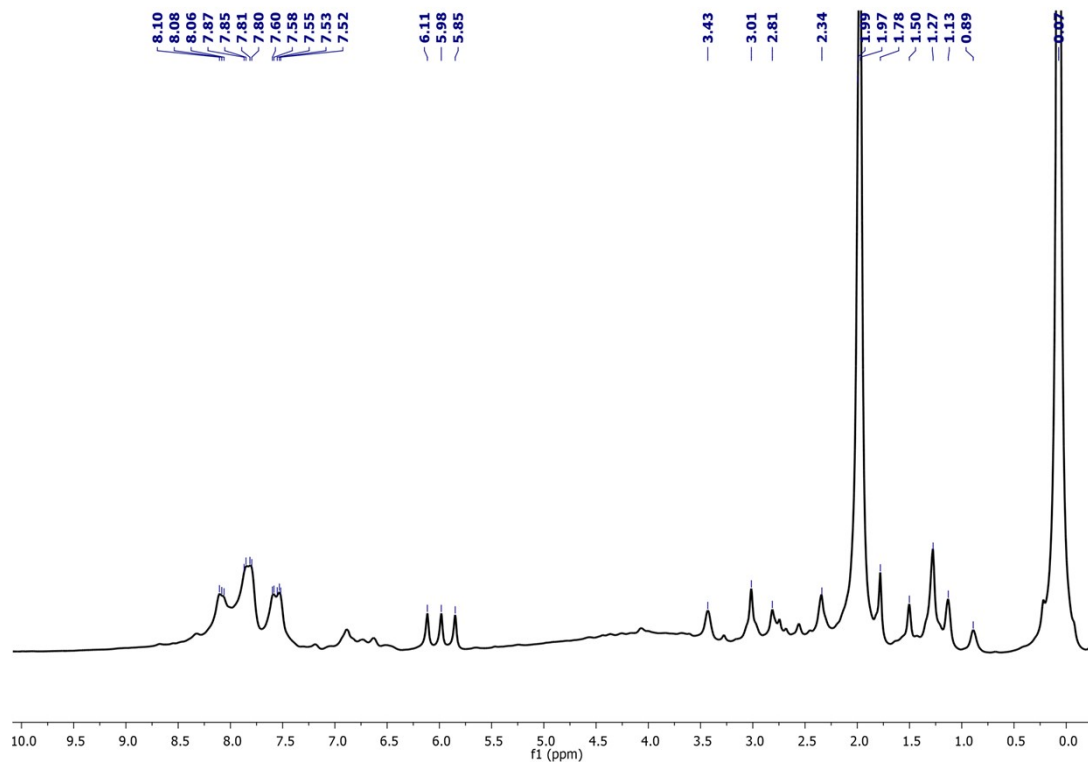


Figure S6. ^1H NMR spectrum of **1** in CD_3CN (500 MHz) at 25 °C.

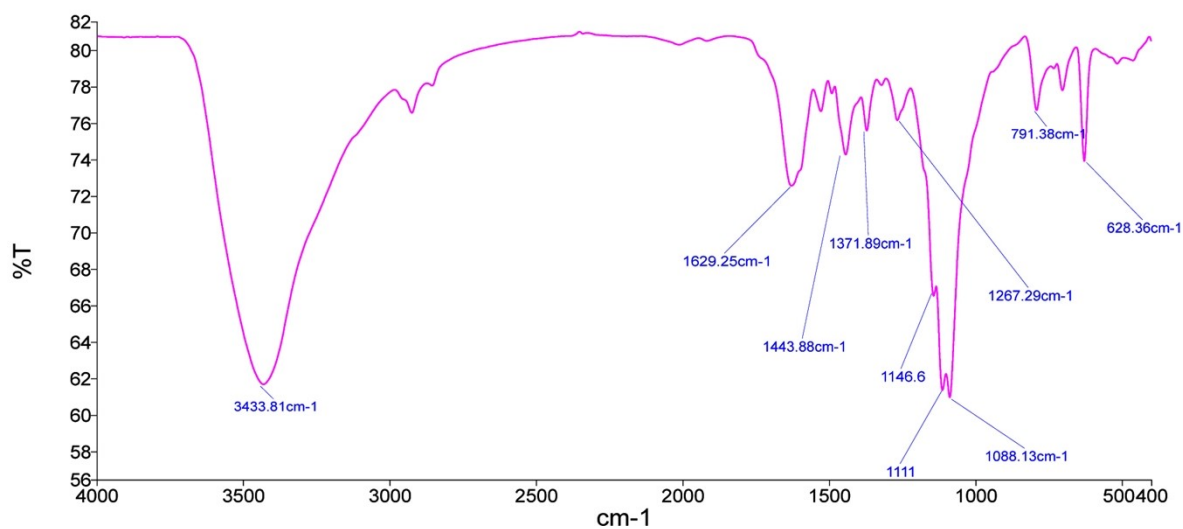


Figure S7. FT-IR spectrum of **1** collected on KBr pellet.

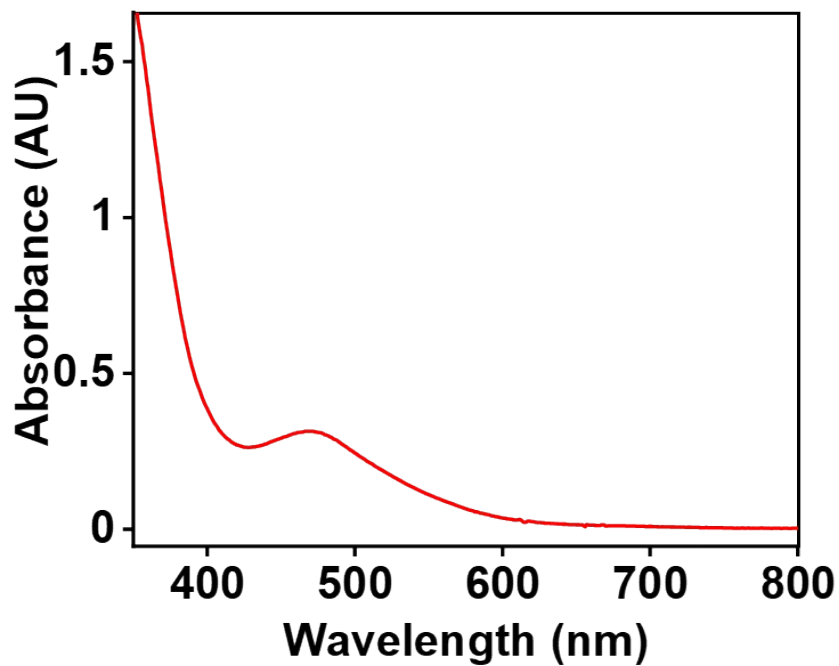


Figure S8. UV-vis spectrum of $[\text{Fe}^{\text{III}}(\text{HL})(\text{CH}_3\text{CN})_2](\text{ClO}_4)_2$ (**1**, 0.25 mM) in acetonitrile at 25 °C. A 1 cm path length cuvette was used during the measurement.

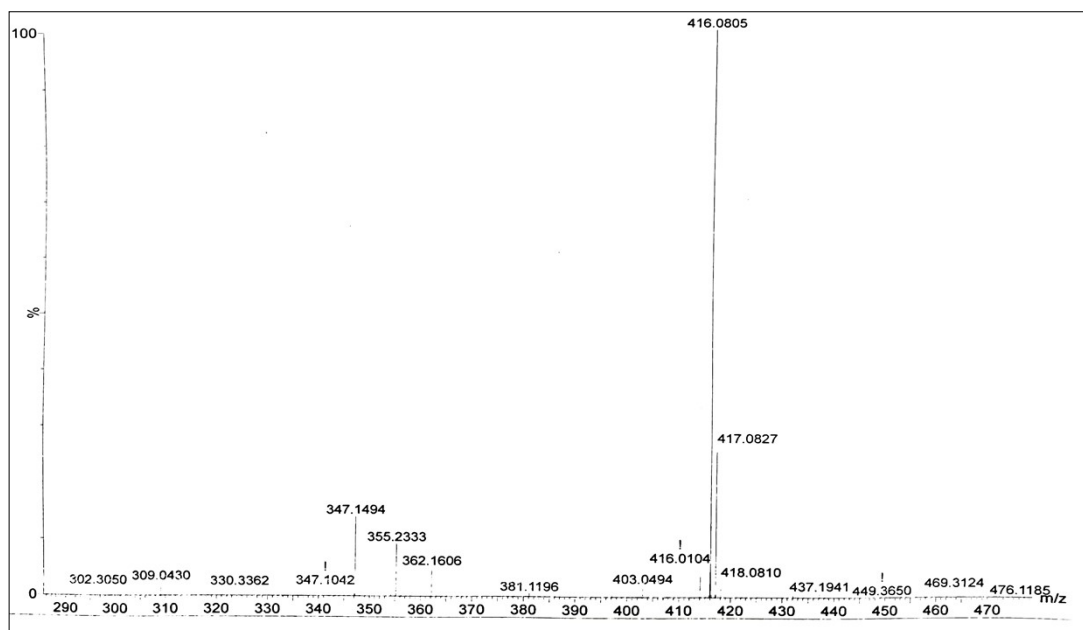


Figure S9. The ESI-mass spectrum of **1a** in acetonitrile (positive ion mode).

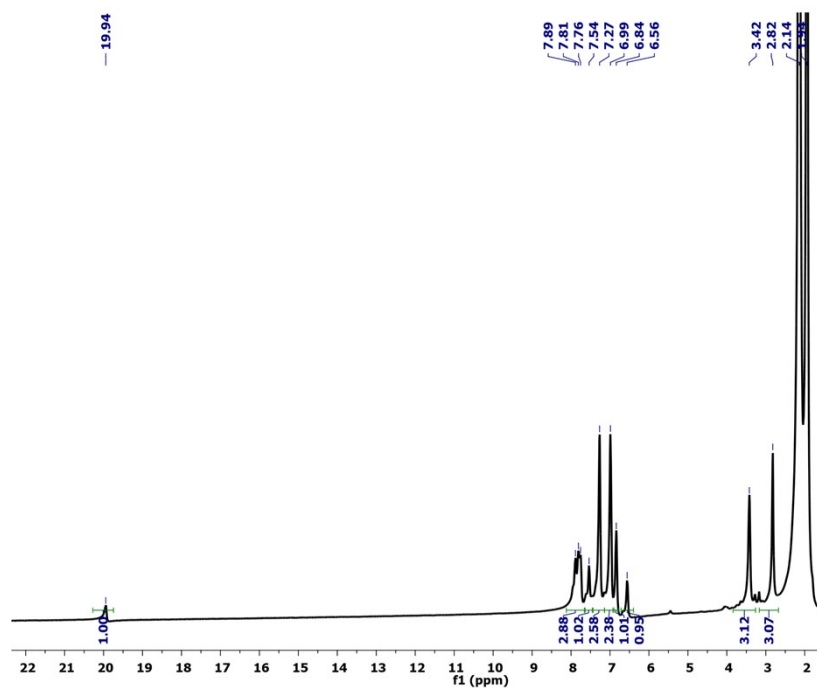


Figure S10. ^1H NMR spectrum of **1a** in CD_3CN (500 MHz) at 25 °C.

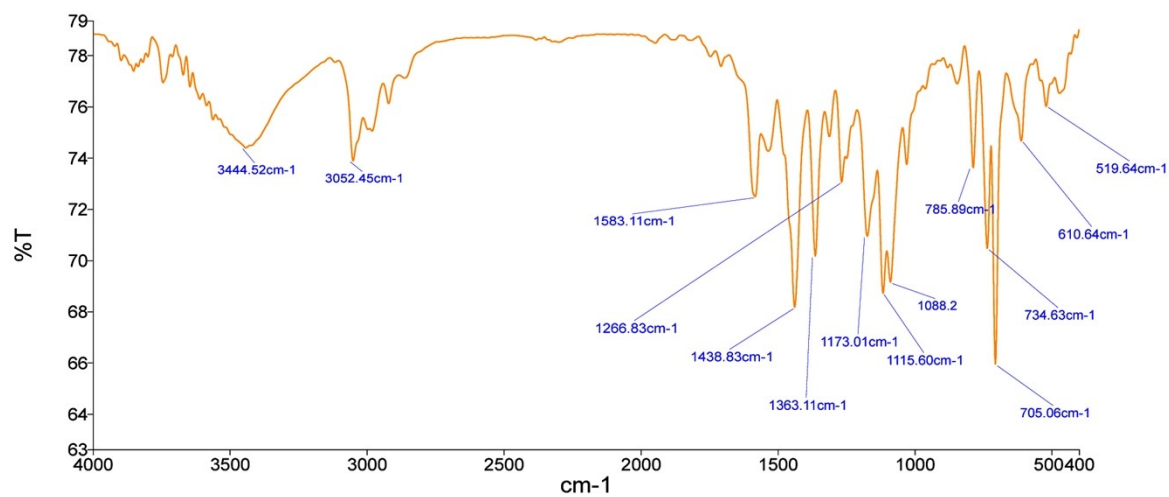


Figure S11. FT-IR spectrum of **1a** obtained on KBr pellet.

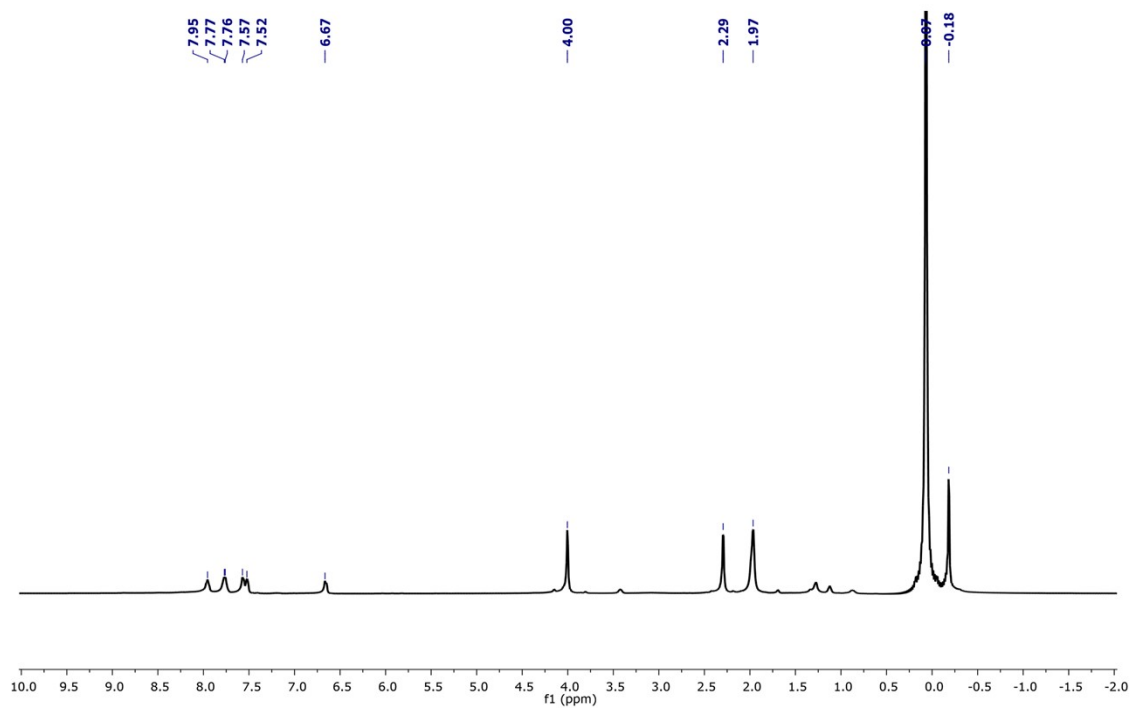


Figure S12. ¹H NMR spectrum of **2** in CD₃CN (400 MHz) at 25 °C.

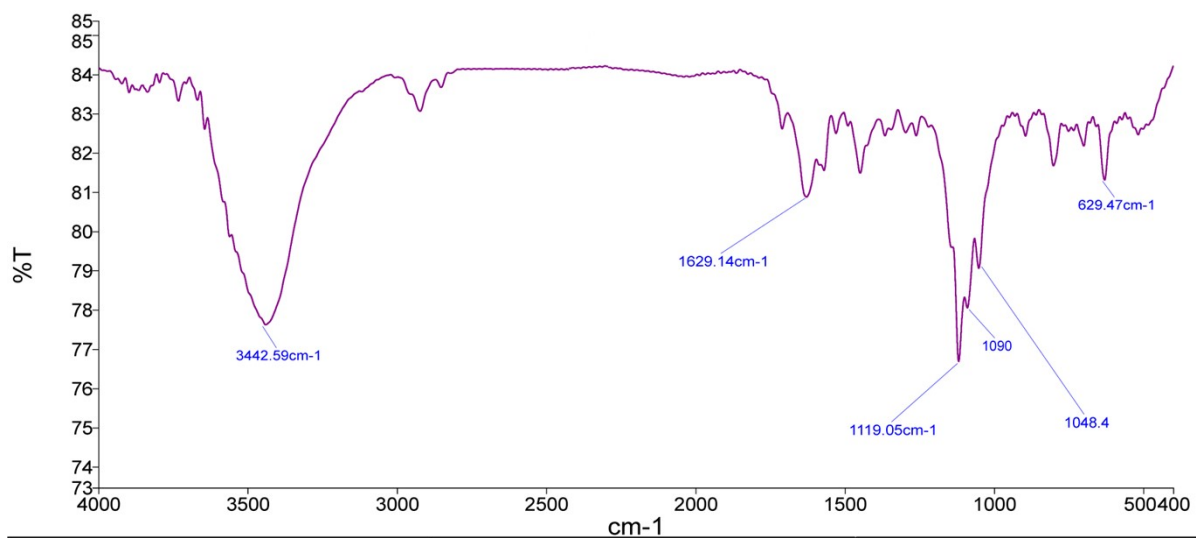


Figure S13. FT-IR spectrum of **2** obtained on KBr pellet.

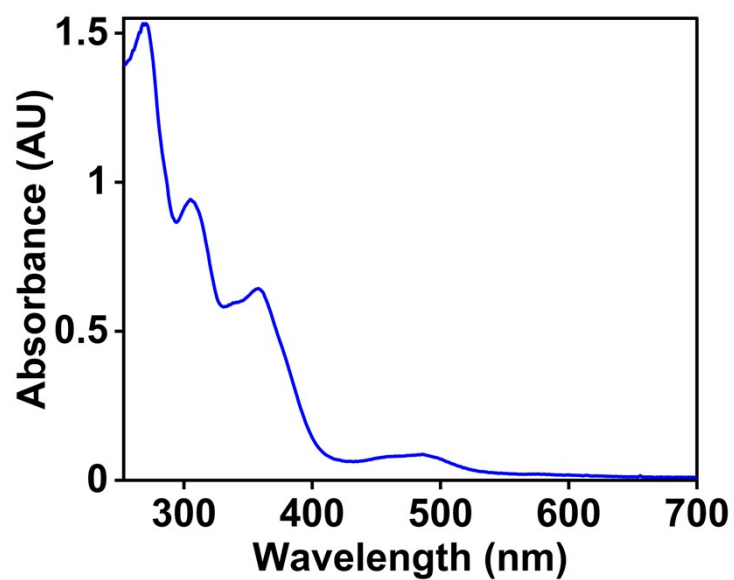


Figure S14. UV-vis spectra of **2** (0.5 mM) in an acetonitrile solution using a 0.1 cm path length cuvette.

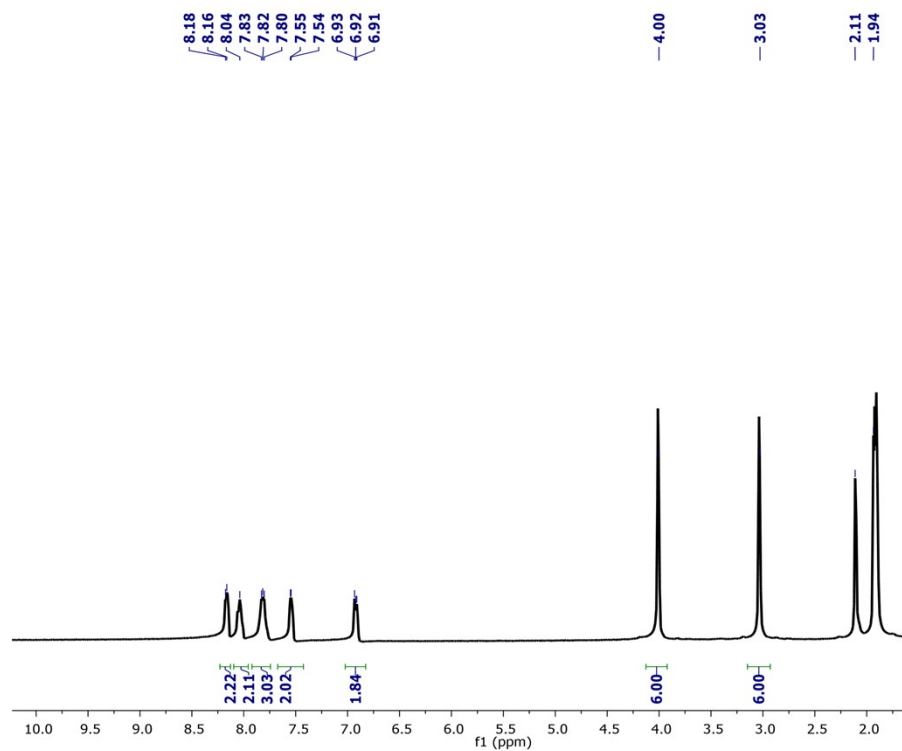


Figure S15. ^1H NMR spectrum of **2a** in CD_3CN (400 MHz) at 25 °C.

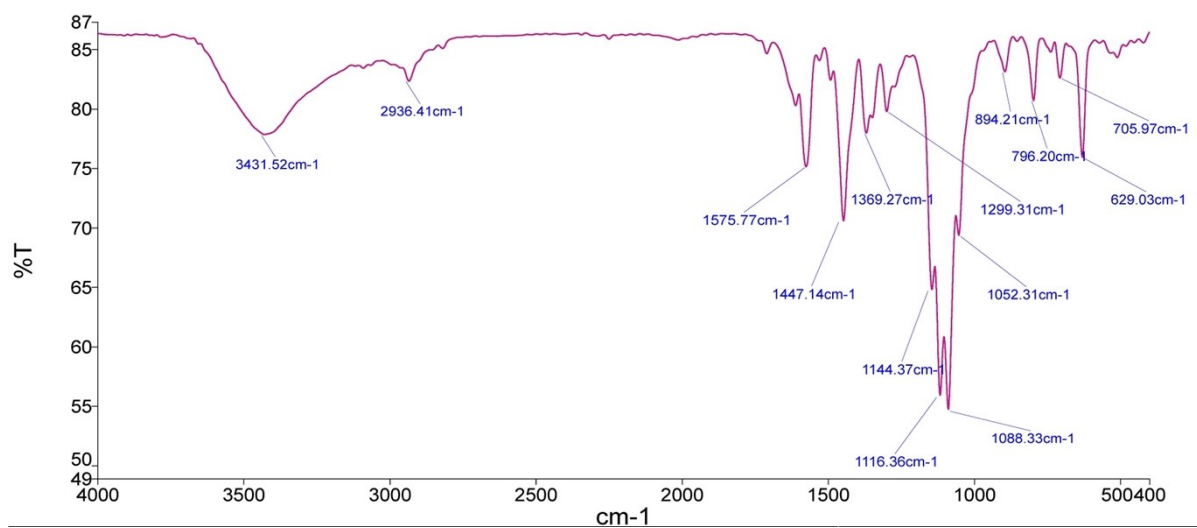


Figure S16. FT-IR spectrum of **2a** collected on KBr pellet.

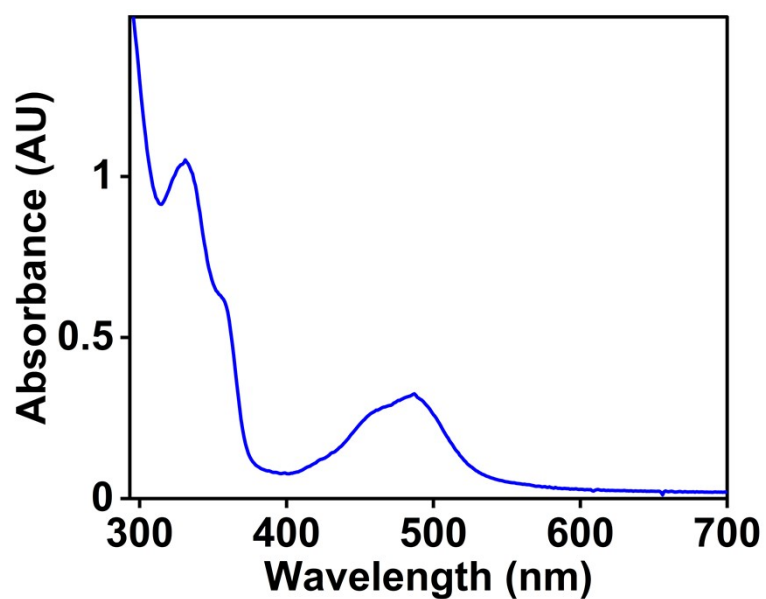


Figure S17. UV-vis spectra of **2a** (0.25 mM) in an acetonitrile solution. A 1 cm pathlength cuvette was used during the measurement.

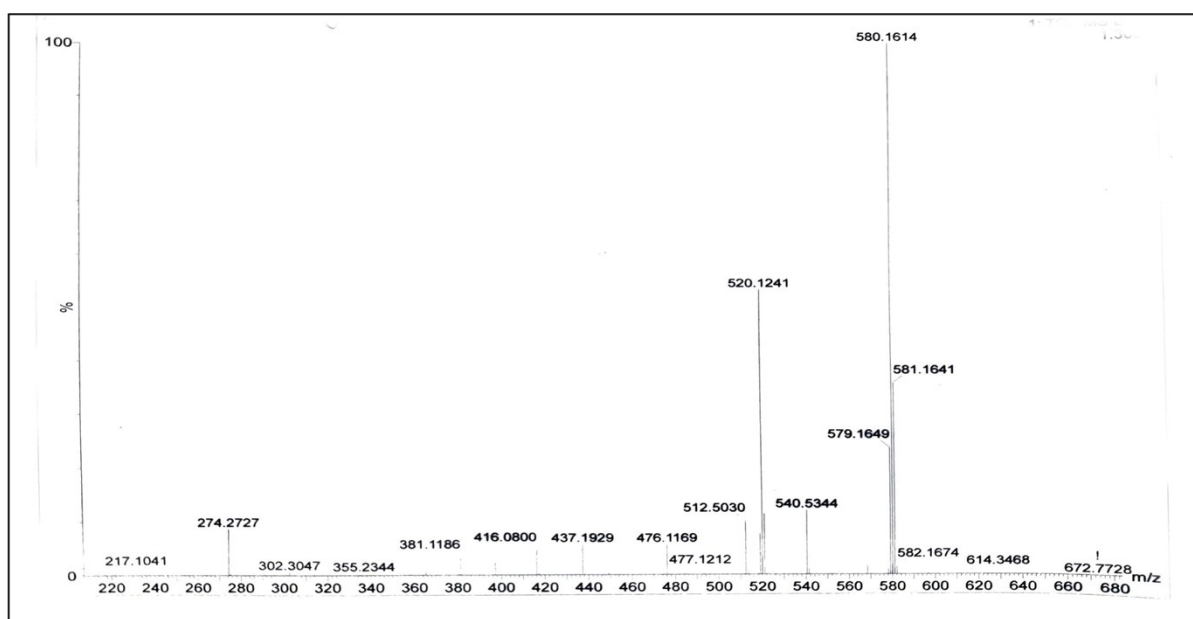


Figure S18. The ESI-mass spectrum of **3a** in acetonitrile (positive ion mode).

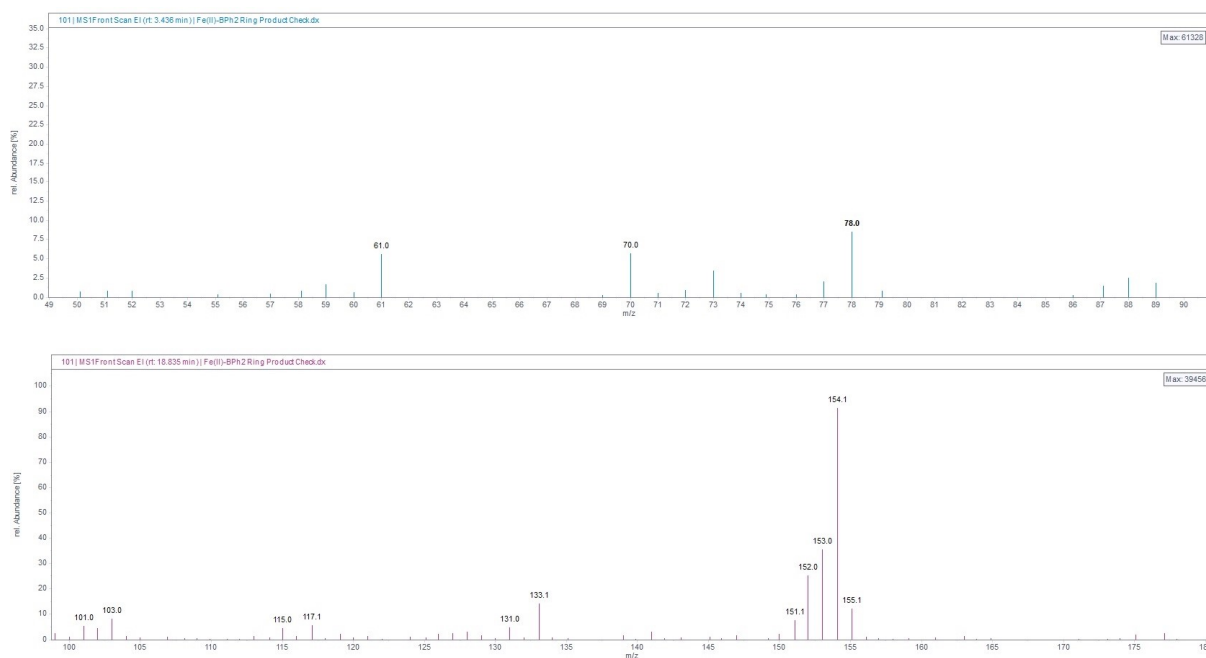
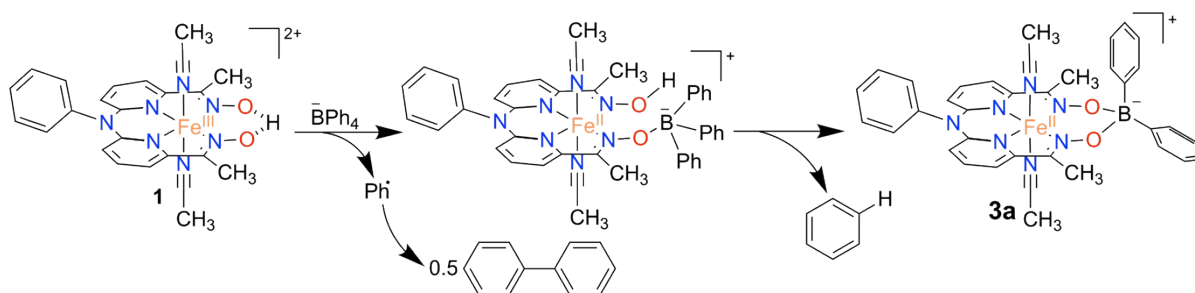


Figure S19. The GC-mass spectrum of the reaction products was obtained from the reaction mixture of **1** and NaBPh₄ in acetonitrile. The above data corresponds to benzene (top) and biphenyl (bottom).



Scheme S2. Proposed mechanism for the formation of **3a** from **1**.

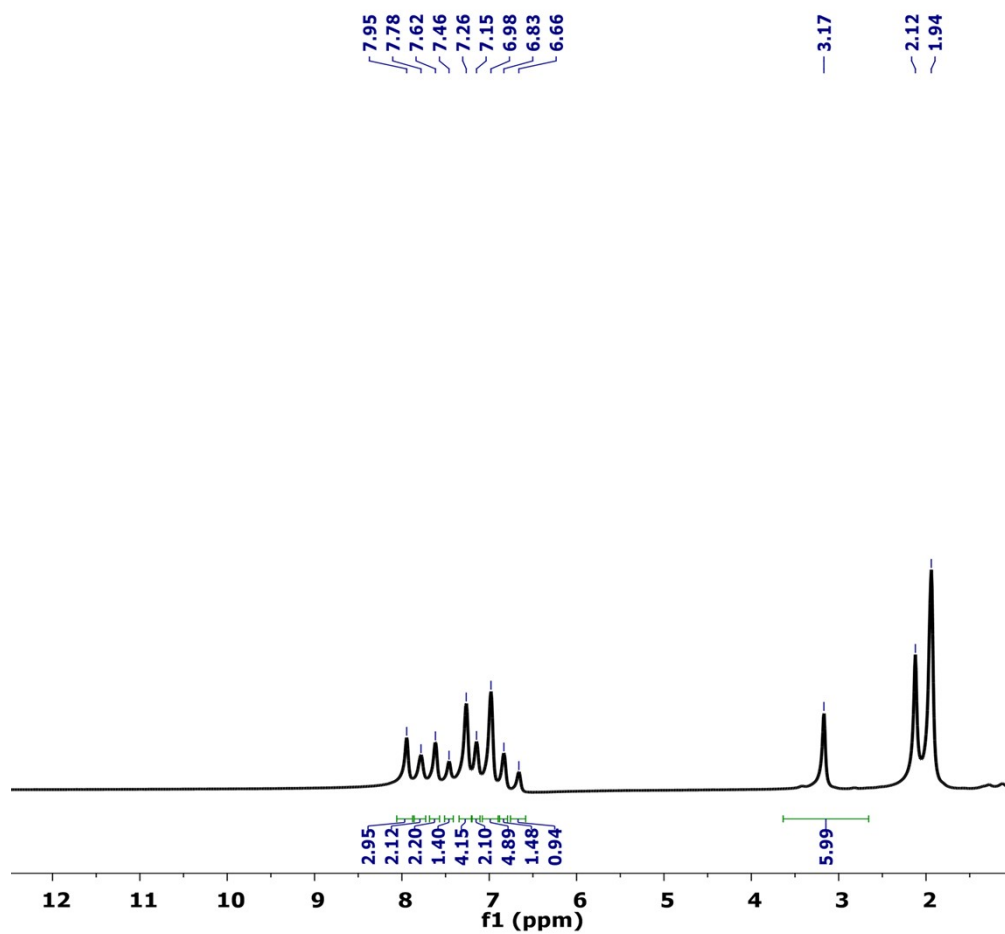


Figure S20. ^1H NMR spectrum of **3a** in CD_3CN (400 MHz) at 25 °C.

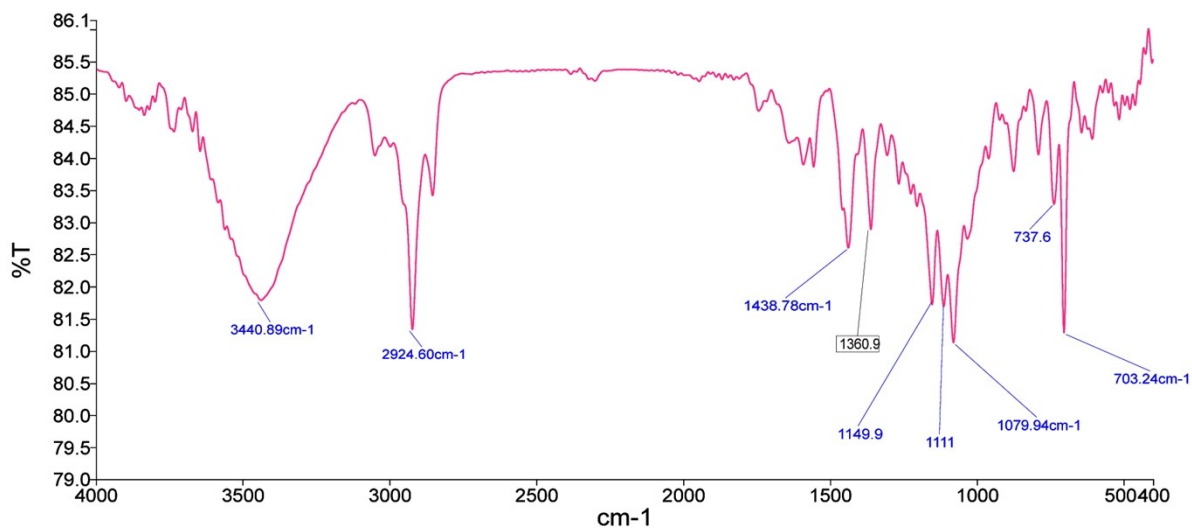


Figure S21. FT-IR spectrum of **2a** recorded on KBr pellet.

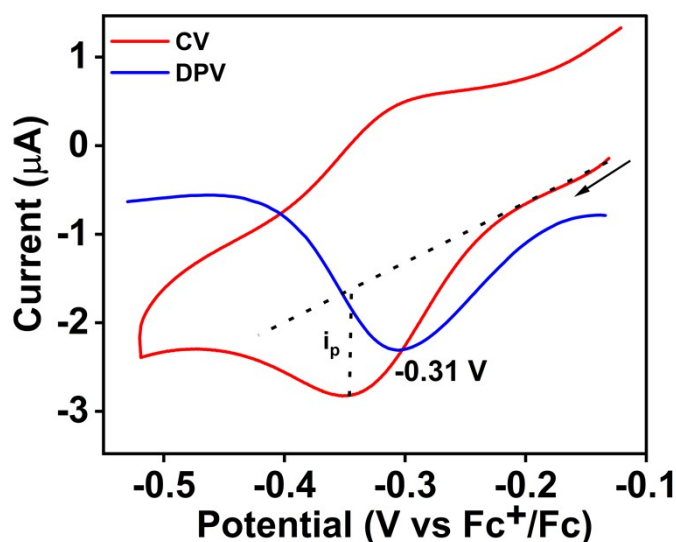


Figure S22. Cyclic voltammogram and differential pulse voltammogram of **1** (0.5 mM) in acetonitrile containing 50 mM $n\text{Bu}_4\text{NPF}_6$ as the supporting electrolyte under N_2 . A 3 mm glassy carbon working electrode, Pt wire counter electrode, and Ag/AgCl in saturated KCl as the reference electrode were used during the measurements. Potential values were reported with respect to the Fc^+/Fc couple. CV data was recorded at a scan rate of 0.1 V/s.

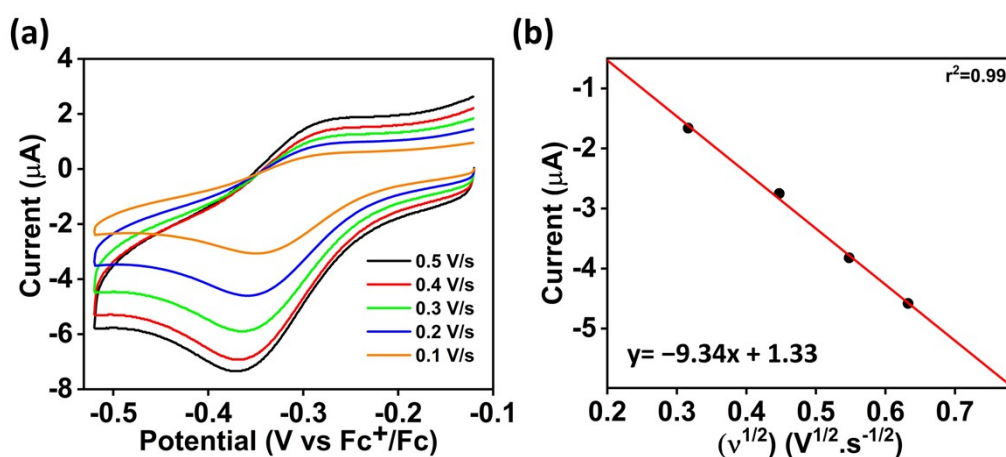


Figure S23. (a) Cyclic voltammogram of **1** (0.5 mM) in acetonitrile in the presence of 50 mM $n\text{Bu}_4\text{NPF}_6$ at different scan rates at 25 °C. A 3 mm glassy carbon working electrode, Pt wire counter electrode, and Ag/AgCl in saturated KCl as the reference electrode were used during the measurements. Potential values were reported with respect to the Fc^+/Fc couple. (b) A plot of cathodic current (i_{pc}) vs. $v^{1/2}$.

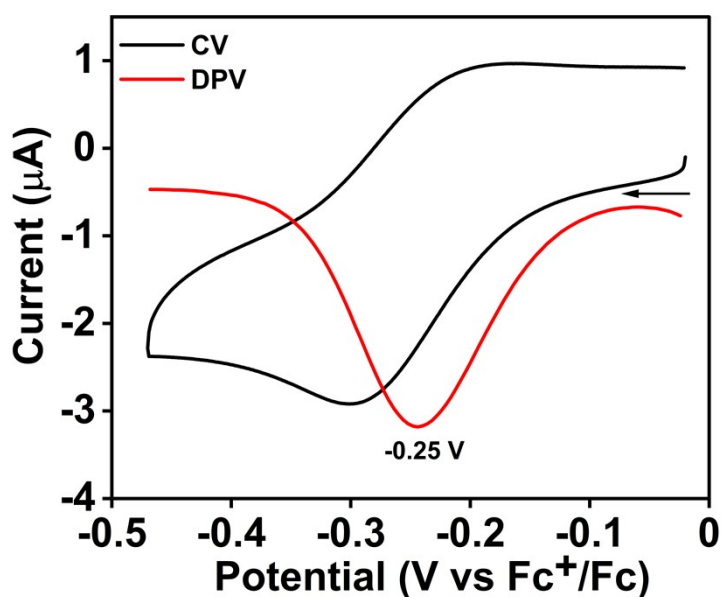


Figure S24. CV and DPV of **2** (0.5 mM) in acetonitrile containing 50 mM $n\text{Bu}_4\text{NPF}_6$ as the supporting electrolyte was obtained upon cathodic scan under N_2 . A 3 mm glassy carbon working electrode, Pt wire counter electrode, and Ag/AgCl in saturated KCl as the reference electrode were used during the measurements. Potential values were reported with respect to the Fc^+/Fc couple. The CV data was recorded at a scan rate of 0.1 V/s.

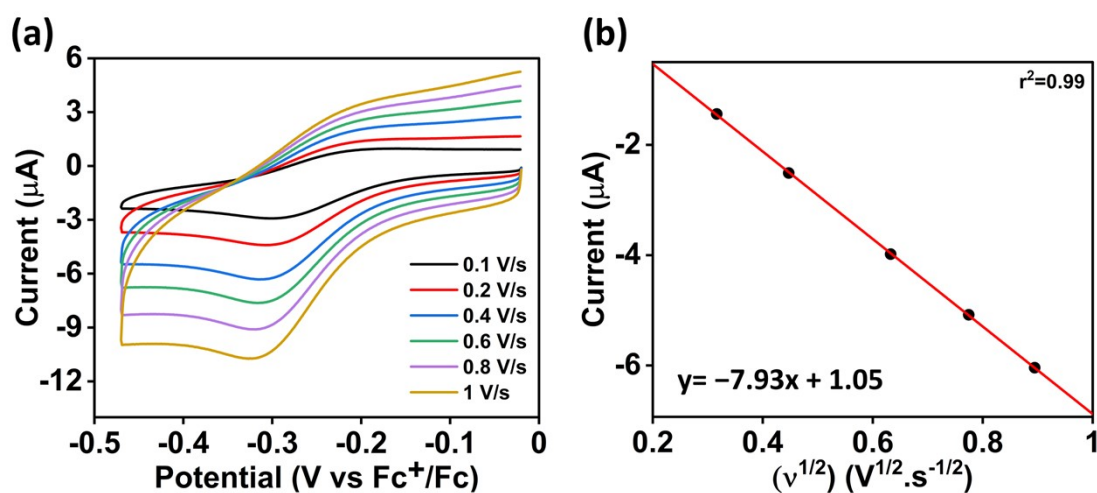


Figure S25. (a) Cyclic voltammogram of **2** (0.5 mM) in acetonitrile in the presence of 50 mM $n\text{Bu}_4\text{NPF}_6$ at different scan rates at 25 °C. A 3 mm glassy carbon working electrode, Pt wire counter electrode, and Ag/AgCl in saturated KCl as the reference electrode were used during the measurements. Potential values were reported with respect to the Fc^+/Fc couple. (b) A plot of cathodic current (i_{pc}) vs $v^{1/2}$.

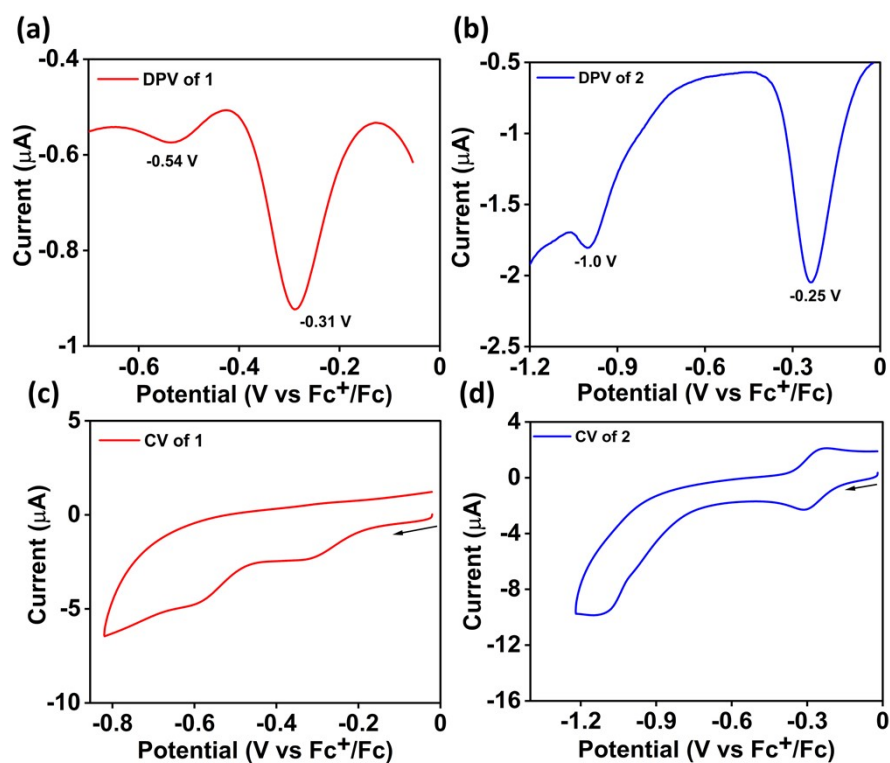


Figure S26. Differential pulse voltammogram of **1** (0.5 mM) (a) and **2** (0.5 mM) (b) under N_2 atmosphere in acetonitrile containing 50 mM nBu_4NPF_6 as the supporting electrolyte. Cyclic voltammogram of **1** (0.5 mM) (c) and **2** (0.5 mM) (d) in acetonitrile containing nBu_4NPF_6 (50 mM) as the supporting electrolyte under the N_2 atmosphere. A scan rate of 0.1 V/s was used during the measurements.

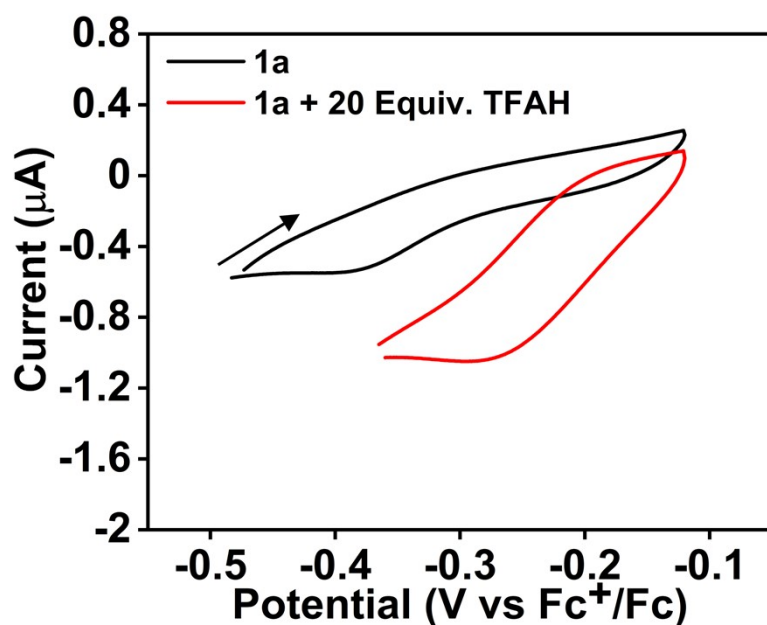


Figure S27. Cyclic voltammogram of **1a** (0.5 mM) in the presence and absence of excess TFAH (20 mM) in acetonitrile containing nBu_4NPF_6 (50 mM) as the supporting electrolyte under the N_2 atmosphere (scan rate 0.005 V/s).

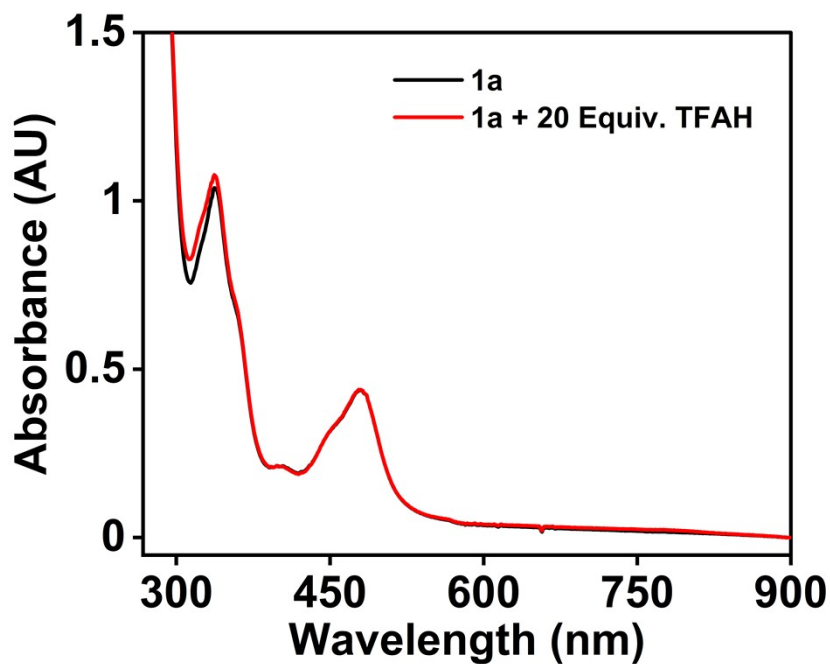


Figure S28. Change of UV-vis spectrum of **1a** (0.25 mM) upon addition of 20 equiv. of TFAH in acetonitrile. A 0.1 cm pathlength cuvette was utilized during the measurements.

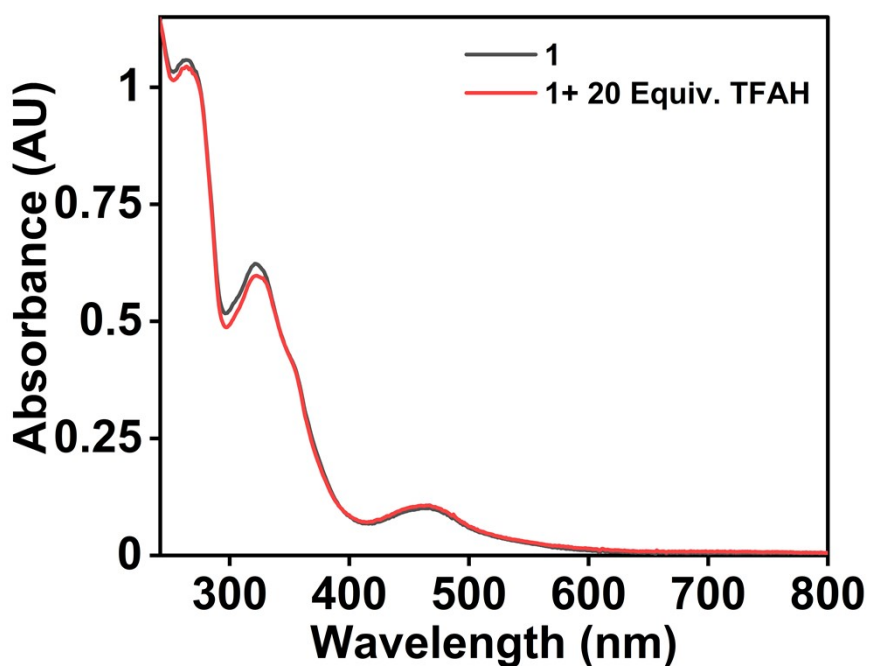


Figure S29. Change of UV-vis spectrum of **1** (0.5 mM) upon addition of 20 equiv. of TFAH in acetonitrile. A 0.1 cm pathlength cuvette was utilized during the measurements.

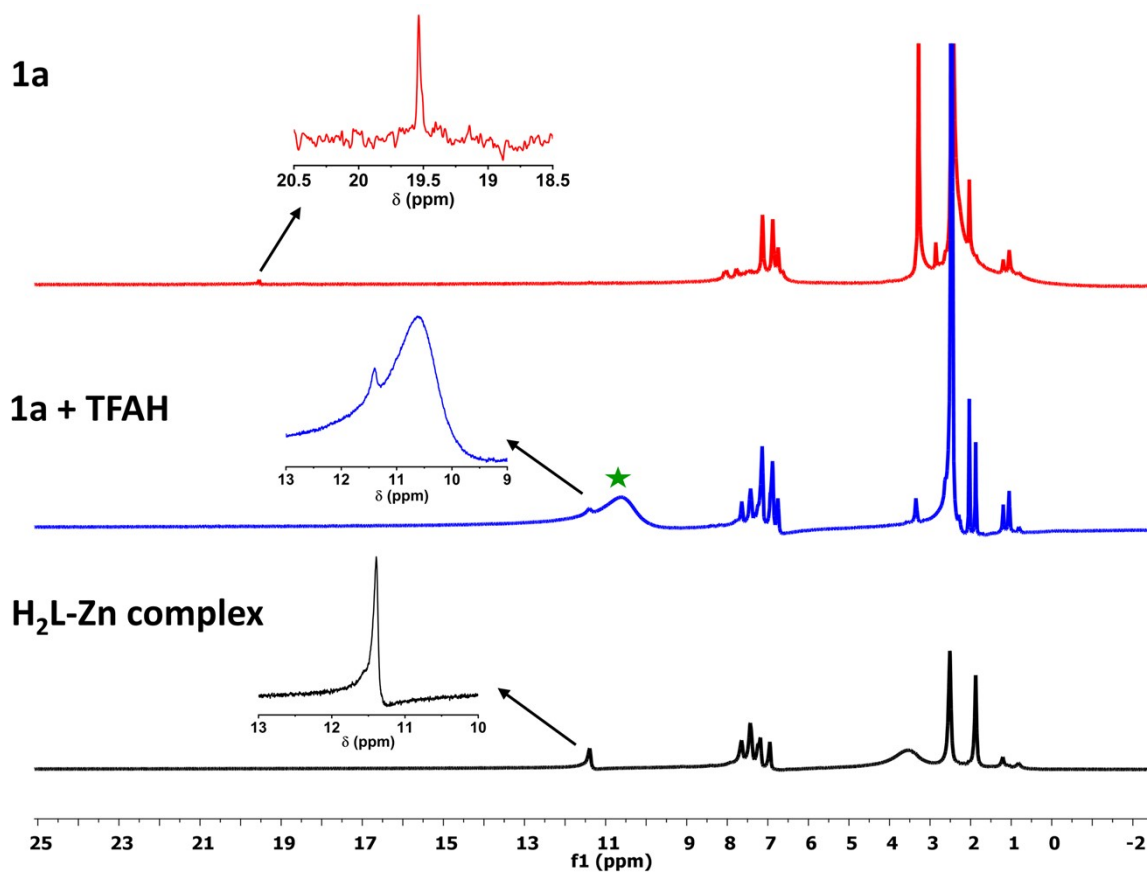


Figure S30. ^1H NMR of **1a**, **1a** + TFAH, and $[\text{Zn}(\text{H}_2\text{L})(\text{Cl})]^+$ in $\text{DMSO-}d_6$ at $25\text{ }^\circ\text{C}$ (400 MHz) (* marked peak corresponds to the acidic proton of excess TFAH).

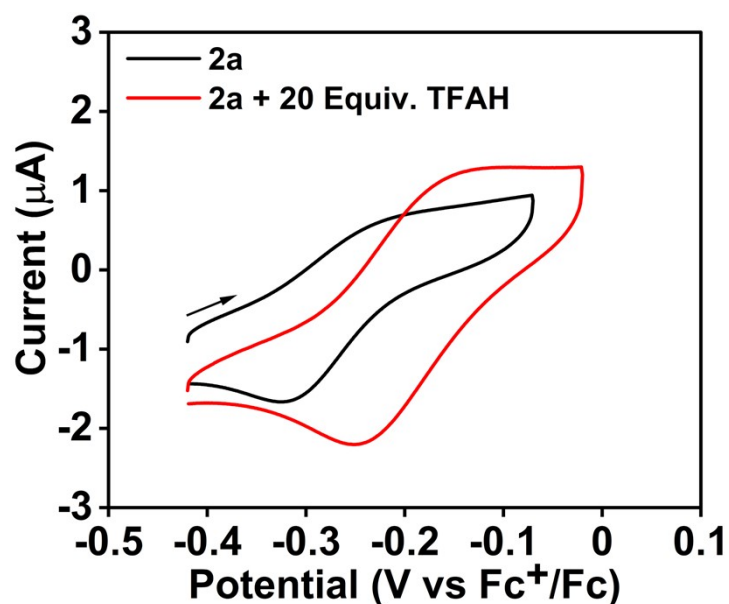


Figure S31. Cyclic voltammogram of **2a** (0.5 mM) in the presence and absence of TFAH (20 mM) in acetonitrile containing $n\text{Bu}_4\text{NPF}_6$ (50 mM) as the supporting electrolyte under a N_2 atmosphere. A scan rate of 0.005 V/s was utilized during the measurements.

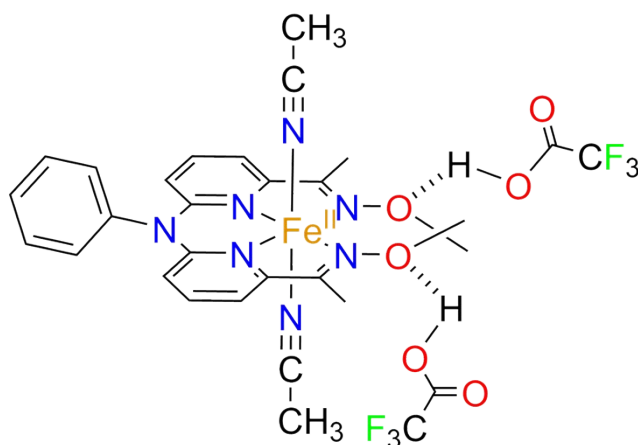


Chart S1. The proposed structure of **2a** in the presence of an excess TFAH.

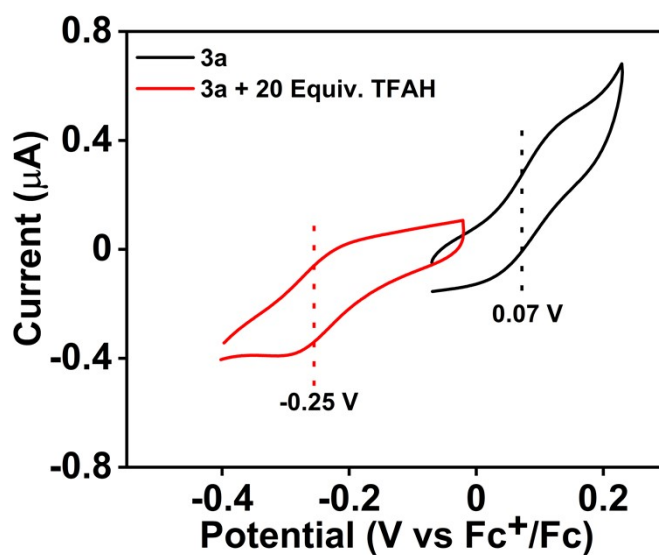


Figure S32. Cyclic voltammogram of **3a** (0.5 mM) in the presence and absence of excess TFAH (20 mM) in acetonitrile containing $n\text{Bu}_4\text{NPF}_6$ (50 mM) as the supporting electrolyte under a N_2 atmosphere. A scan rate of 0.005 V/s was utilized during the measurements.

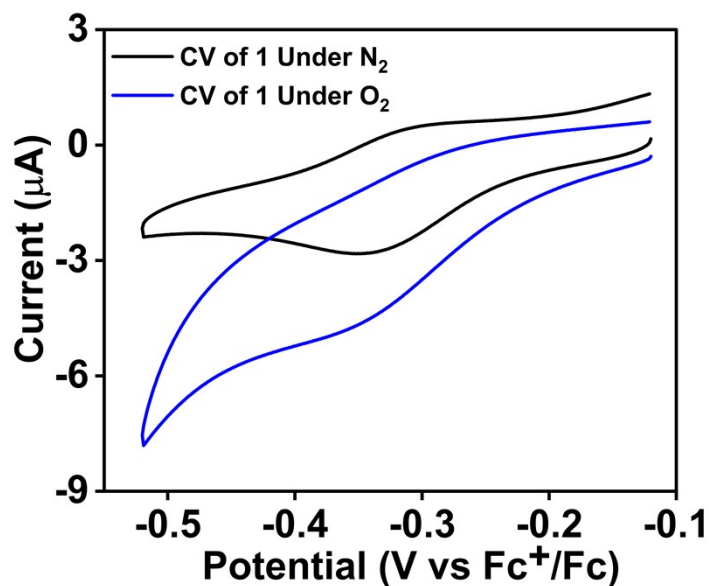


Figure S33. Cyclic voltammogram of **1** (0.5 mM) under N_2 (black) and saturated O_2 (Blue) in acetonitrile containing 50 mM nBu_4PF_6 as the supporting electrolyte. A scan rate of 0.1 V/s was utilized during the measurements.

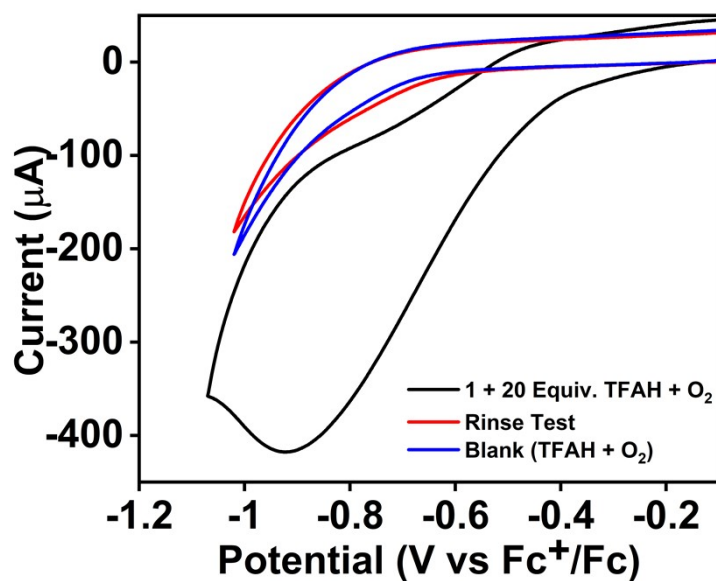


Figure S34. A rinse test experiment was performed using complex **1** (0.5 mM) in an oxygen-saturated acetonitrile solution containing 10 mM TFAH and 50 mM nBu_4NPF_6 as a supporting electrolyte at 6 V/s scan rate. CV response was recorded in the presence of **1** (black) and in the absence of **1** (blue) in oxygen-saturated acetonitrile solution containing 50 mM of nBu_4NPF_6 as the supporting electrolyte and 10 mM TFAH. After the CV scan with **1**, the working electrode was rinsed with acetonitrile, and a CV response (red trace) was recorded again in an oxygen-saturated acetonitrile solution containing 10 mM TFAH.

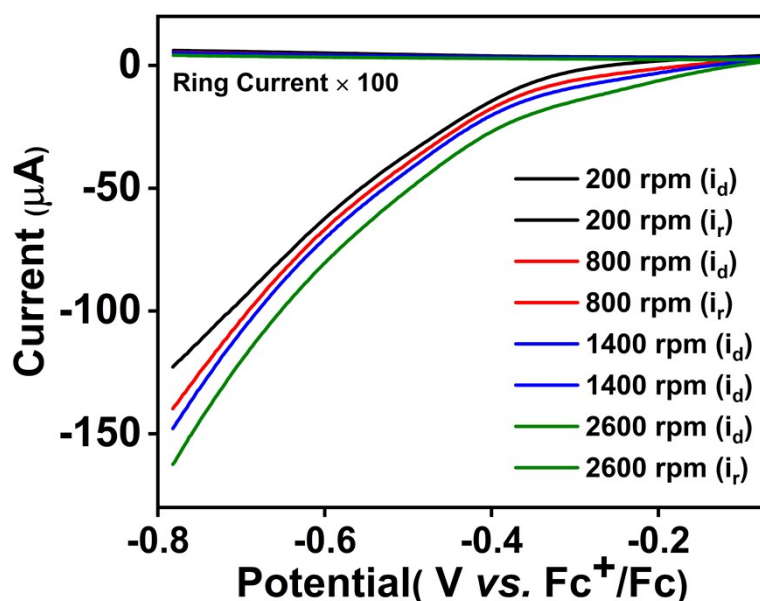


Figure S35. LSV of the RRDE experiments at different rotation rates. A 0.5 mM of **1** in the presence of 10 mM of TFAH in an oxygen-saturated acetonitrile solution was used during the measurements. Ring potential was held at 0.81 V vs. Fc^+/Fc . A glassy carbon disk/Pt ring working electrode, Pt wire counter electrode, and Ag/AgCl in saturated KCl as the reference electrode were used during the measurements.

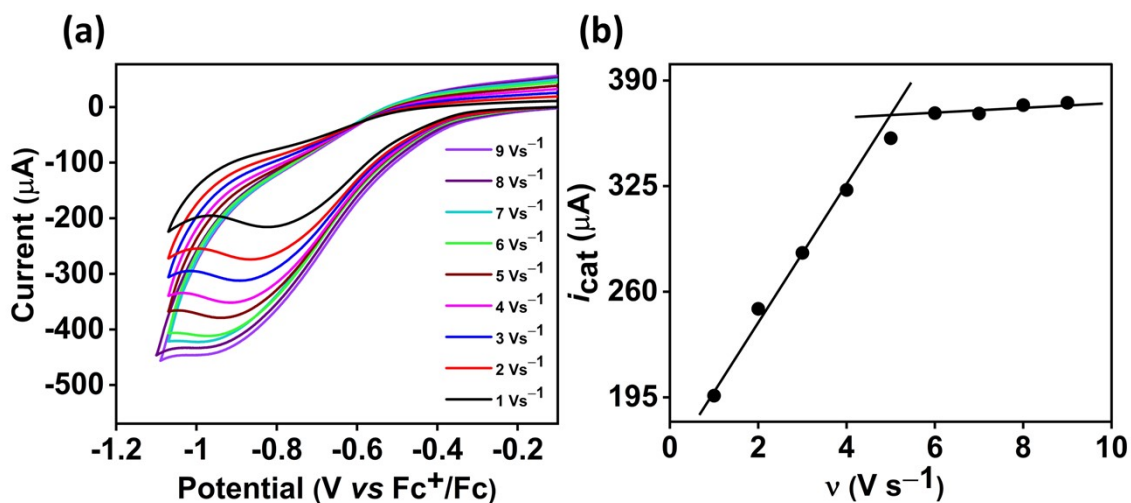


Figure S36. (a) Cyclic voltammogram of **1** (0.5 mM) in an oxygen-saturated acetonitrile solution containing 50 mM $n\text{Bu}_4\text{NPF}_6$ as the supporting electrolyte and 10 mM TFAH as the proton source at different scan rates at 25 °C. A 3 mm glassy carbon working electrode, Pt wire counter electrode, and Ag/AgCl in saturated KCl as the reference electrode were used during the measurements. Potential values were reported with respect to the Fc^+/Fc couple. (b) A plot of catalytic current (i_{cat}) vs. scan rate (ν).

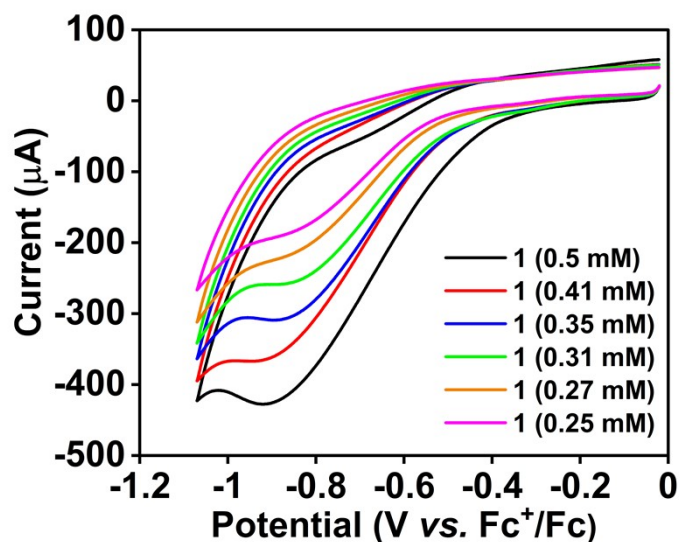


Figure S37. Cyclic voltammogram of **1** at a variable concentration of the complex (0.25-0.5 mM) in an oxygen-saturated acetonitrile solution containing 10 mM TFAH and 50 mM ⁿBu₄NPF₆ at 25 °C. A scan Rate of 6 V/s was used during the measurements.

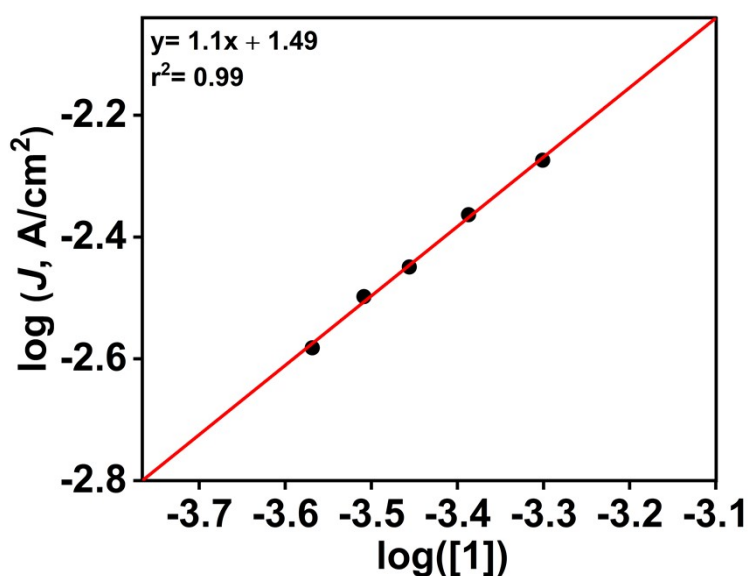


Figure S38. Plots of $\log(J, \text{A}/\text{cm}^2)$ vs. $\log[1]$ in oxygen-saturated acetonitrile solution containing 10 mM TFAH and 50 mM ⁿBu₄NPF₆. For this plot, the corresponding cyclic voltammograms were measured at a scan rate of 6 V s⁻¹.

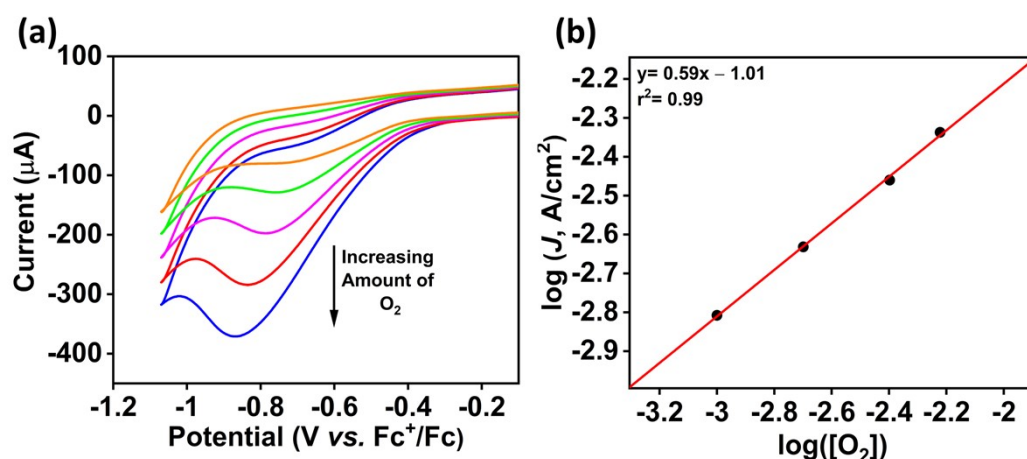


Figure S39. (a) Cyclic voltammogram of **1** (0.5 mM) in acetonitrile containing 10 mM TFAH and 50 mM $n\text{Bu}_4\text{NPF}_6$ with an increasing concentration of O_2 at 25 °C. The cyclic voltammograms were recorded at a scan rate of 6 V/s. (b) Plots of $\log(J, \text{A}/\text{cm}^2)$ vs. $\log([\text{O}_2])$ for **1**.

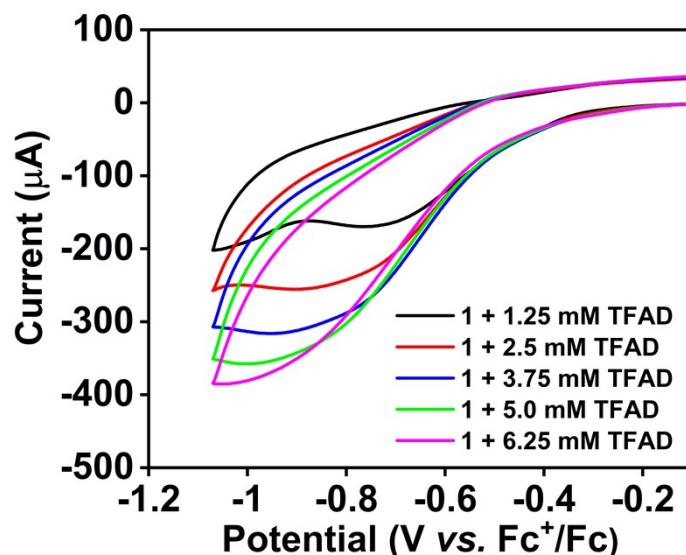


Figure S40. Cyclic voltammogram of **1** (0.5 mM), measured at different concentrations of TFAD (1.25-6.25 mM) in oxygen-saturated acetonitrile solution containing 50 mM $n\text{Bu}_4\text{NPF}_6$ as the supporting electrolyte at a scan rate of 6 V/s at 25 °C.

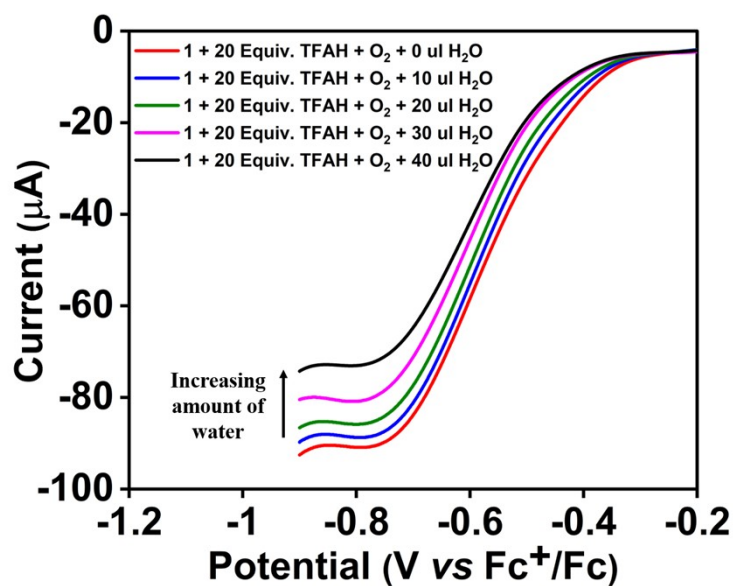


Figure S41. Linear sweep voltammogram (LSV) of **1** (0.5 mM) in oxygen-saturated acetonitrile solution containing 10 mM TFAH as the proton source and 50 mM ⁿBu₄NPF₆ as the supporting electrolyte with an increasing concentration of H₂O at 25 °C. A scan rate of 0.1 V/s was used for the measurements.

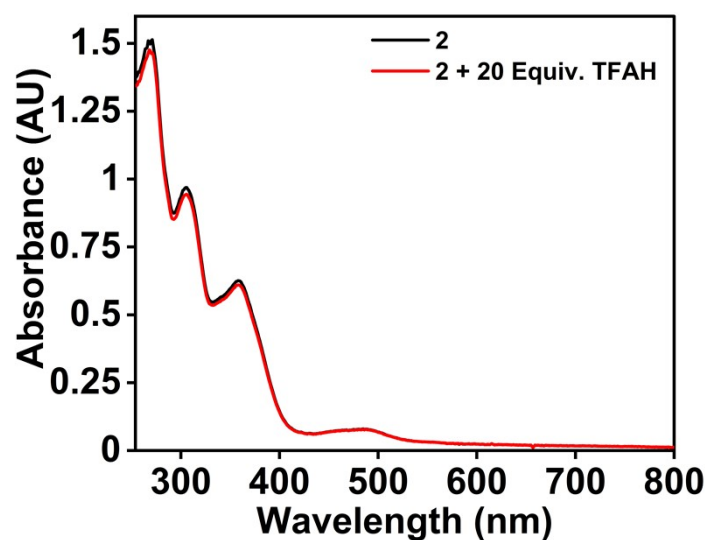


Figure S42. Change of UV-vis spectrum of **2** (0.5 mM) upon addition of 20 equiv. TFAH (0.1 cm pathlength cuvette) in acetonitrile at 25 °C. The data was recorded using a 0.1 cm pathlength cuvette.

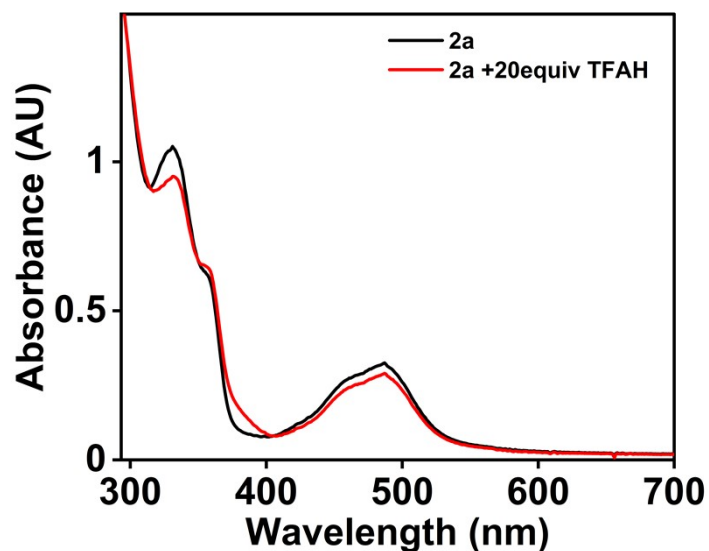


Figure S43. Change of UV-vis spectrum of **2a** (0.5 mM) upon addition of 20 equiv. TFAH in acetonitrile at 25 °C. The data was recorded using a 0.1 cm pathlength cuvette.

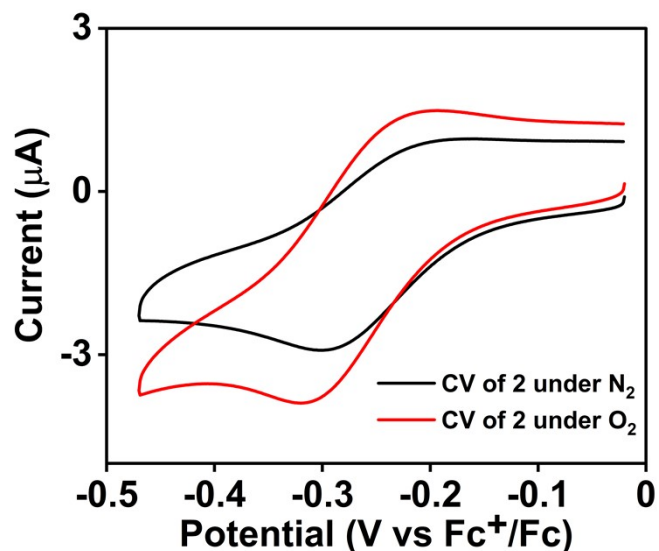


Figure S44. Cyclic voltammogram of **2** (0.5 mM) under N_2 (black track) and in oxygen-saturated acetonitrile solution (red trace) containing 50 mM $n\text{Bu}_4\text{NPF}_6$ as the supporting electrolyte at 25 °C. The data was recorded at a scan rate of 0.1 V/s.

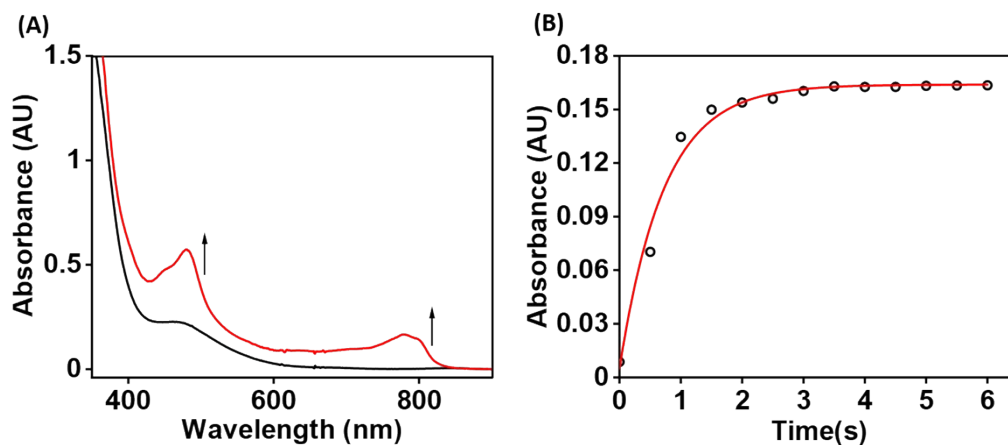


Figure S45. (a) Change of UV-vis spectrum observed upon addition of one equiv. of Fc^* to an acetonitrile solution of **1** (0.25 mM) at 25 °C. (b) Change of absorbance at 780 nm upon addition of Fc^* to an acetonitrile solution of **1** (0.25 mM) at 25 °C.

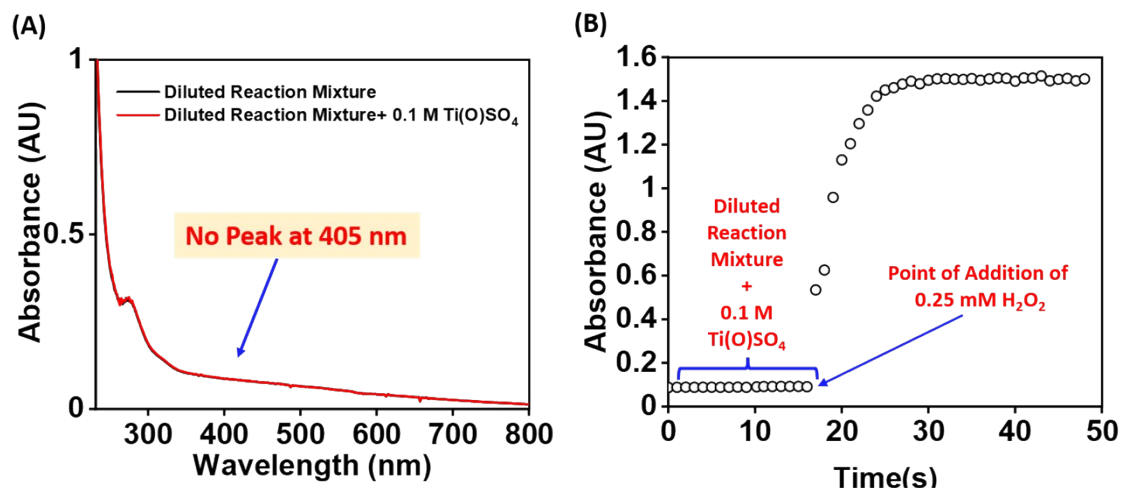


Figure S46. (a) Change of UV-vis spectrum upon addition of 0.1 M $\text{Ti}(\text{O})\text{SO}_4$ to the diluted reaction mixture of the reaction solution containing catalytic amounts of **1**, TFAH, and the ORR product (s). (b) Change of absorbance at 405 nm upon addition of 0.1 M $\text{Ti}(\text{O})\text{SO}_4$ to the reaction solution (**1** + TFAH + Fc^* + O_2) and then H_2O_2 . The addition of H_2O_2 to the reaction mixture causes an immediate increase in absorbance at 405 nm.

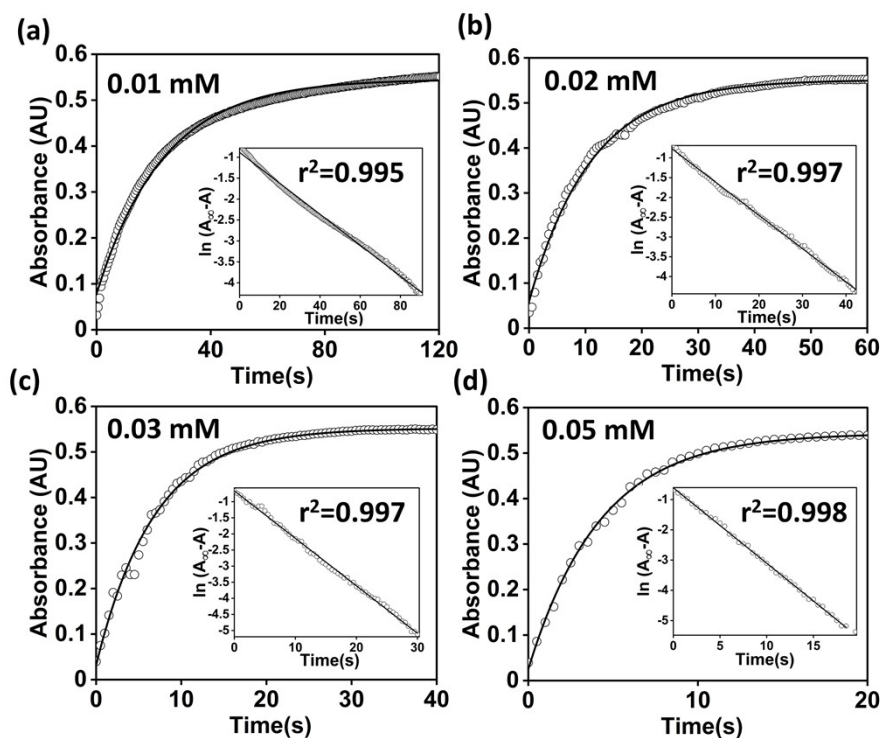


Figure S47. Change of absorbance in the UV-vis spectrum at 780 nm for the reaction of Fc^* (1 mM) with O_2 (8.1 mM) in the presence of 20 mM of TFAH and **1** (0.01 mM (a), 0.02 mM

(b), 0.03 mM (c), 0.05 mM (d)). [Inset: Plots of $\ln(A_\infty - A)$ vs. time (s) at different concentrations of **1** for the determination of k_{obs} values].

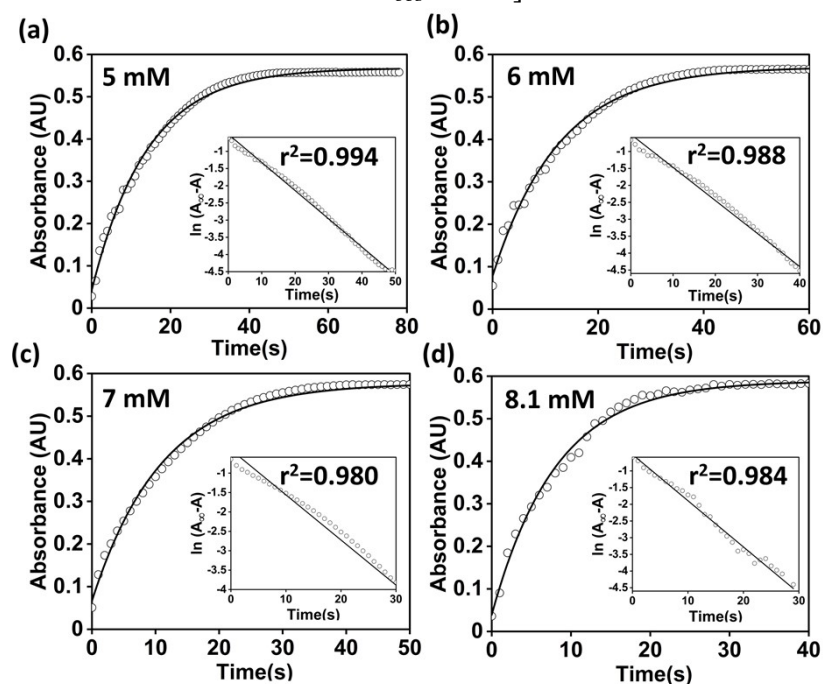


Figure S48. Change of absorbance in the UV-vis spectrum at 780 nm for the reaction of Fc* (1 mM) with O₂ (5 mM (a), 6 mM (b), 7 mM (c), 8.1 mM (d)) in the presence of 20 mM of TFAH and 0.02 mM of **1**. [Inset: Plots of $\ln(A_\infty - A)$ vs time (s) at different concentrations of O₂ for the determination of k_{obs} values]

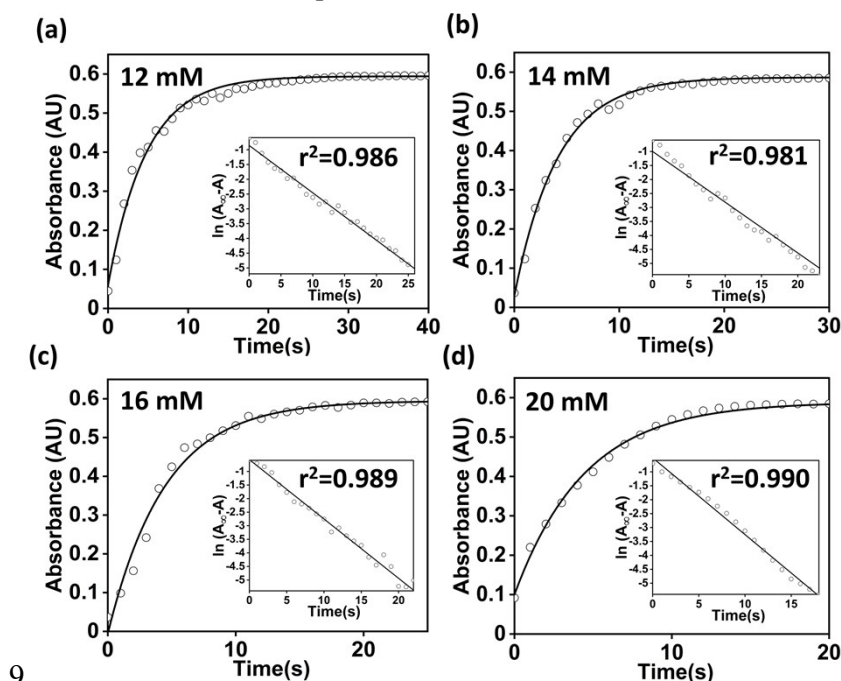


Figure S49. Change of absorbance in the UV-vis spectrum at 780 nm for the reaction of Fc* (1 mM) with O₂ (8.1 mM) in the presence of 0.02 mM of **1** and TFAH (12 mM (a), 14 mM (b), 16 mM (c), 20 mM (d)). [Inset: Plots of $\ln(A_\infty - A)$ vs. time (s) at different concentrations of TFAH for the determination of k_{obs} values]

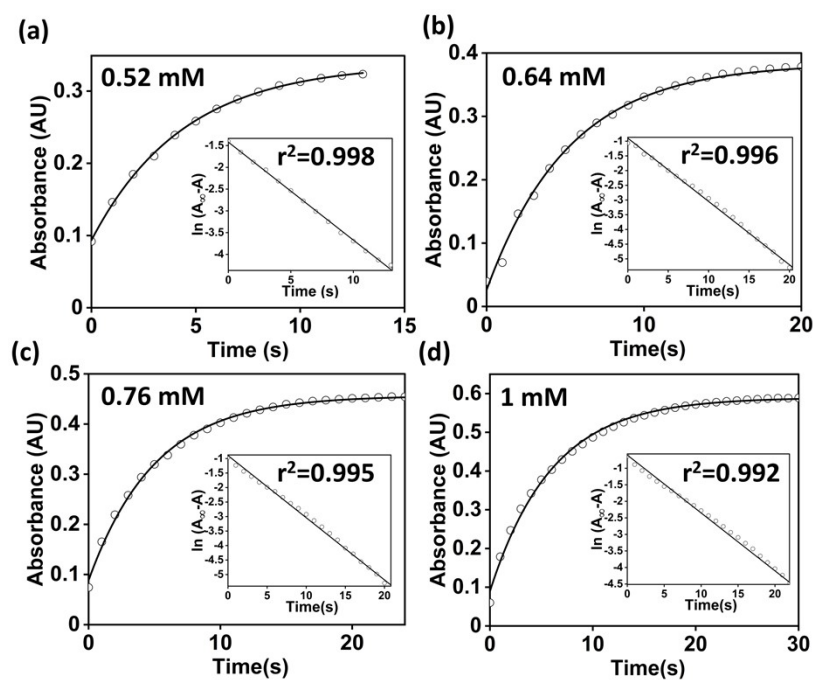


Figure S50. Change of absorbance in the UV-vis spectrum at 780 nm for the reaction of Fc* (0.52 mM (a), 0.64 mM (b), 0.76 mM (c), 1.0 mM (d)) with O₂ (8.1 mM) in the presence of 20 mM of TFAH and 0.02 mM of 1. [Inset: Plots of ln(A_∞-A) vs time (s) at different concentrations of Fc* for the determination of k_{obs} values]

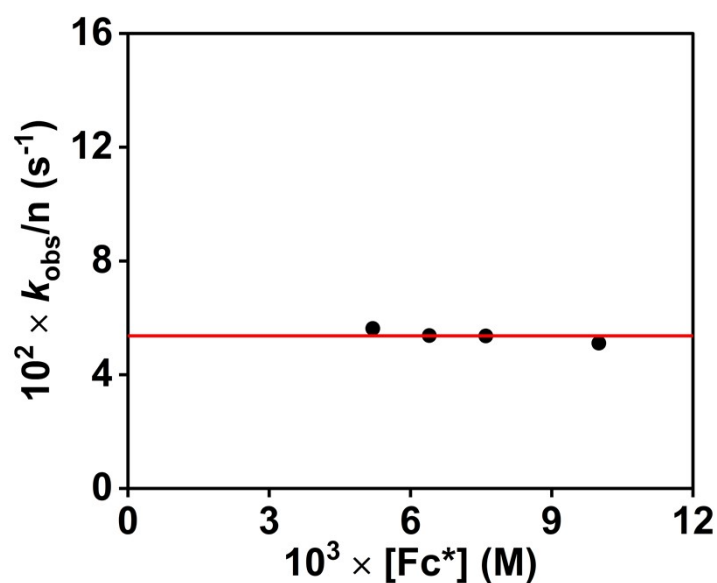


Figure S51. A plot of k_{obs} vs. $[\text{Fc}^*]$ at a fixed concentration of 1 (0.02 mM), TFAH (20 mM), and O₂ (8.1 mM) at 25 °C.

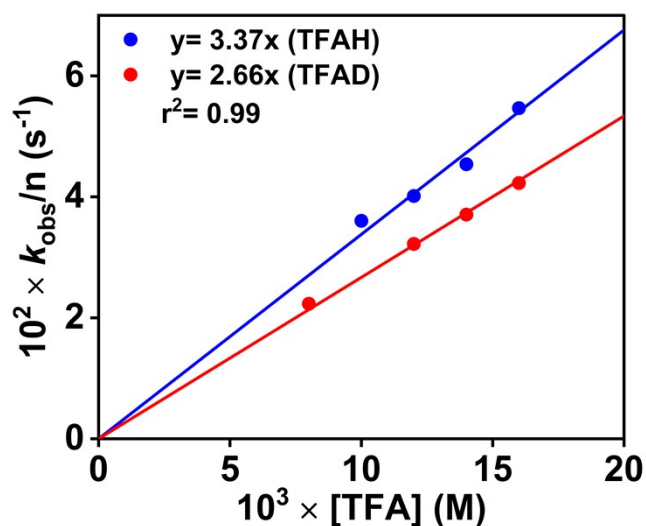


Figure S52. A plot of $k_{\text{obs}} \text{ (s}^{-1}\text{)}$ vs. concentration of TFAH or TFAD for the reaction of **1** with O_2 and Fc^* in acetonitrile at 25 °C.

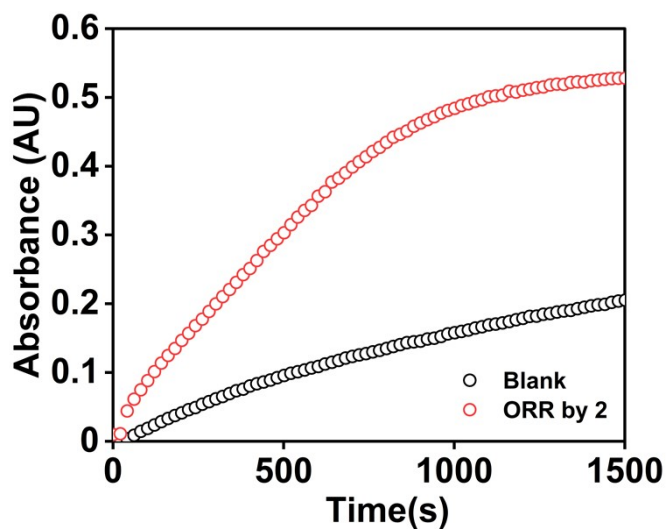


Figure S53. ORR by **2** (0.02 mM) in acetonitrile and the corresponding blank experiments under a similar reaction condition ($\text{Fc}^* = 1 \text{ mM}$, $\text{TFAH} = 20 \text{ mM}$, $\text{O}_2 = 8.1 \text{ mM}$).

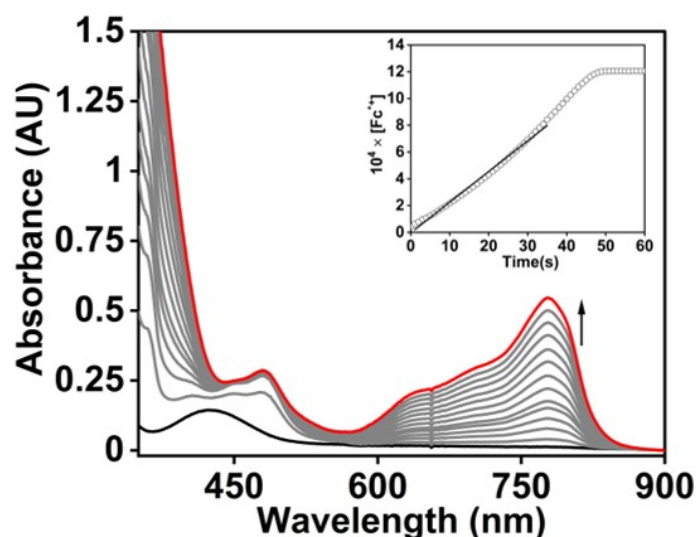


Figure S54. Change of the UV-vis spectrum of **3** (0.02 mM) in an oxygen-saturated acetonitrile solution (8.1 mM) in the presence of 1 mM Fc* and 20 mM TFAH at 25 °C. The inset figure shows the formation of Fc*+ at 780 nm

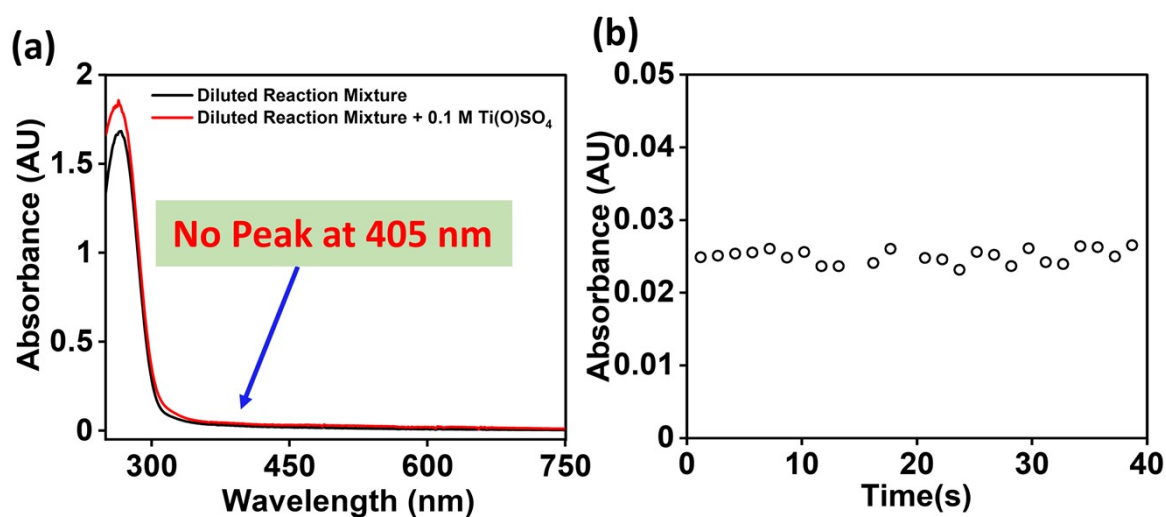


Figure S55. (a) Change of UV-vis spectrum upon addition of 0.1 M Ti(O)SO₄ to the diluted catalytic reaction mixture. (b) Change of absorbance at 405 nm upon addition of 0.1 M Ti(O)SO₄ to the reaction solution (**3** + TFAH + Fc* + O₂).

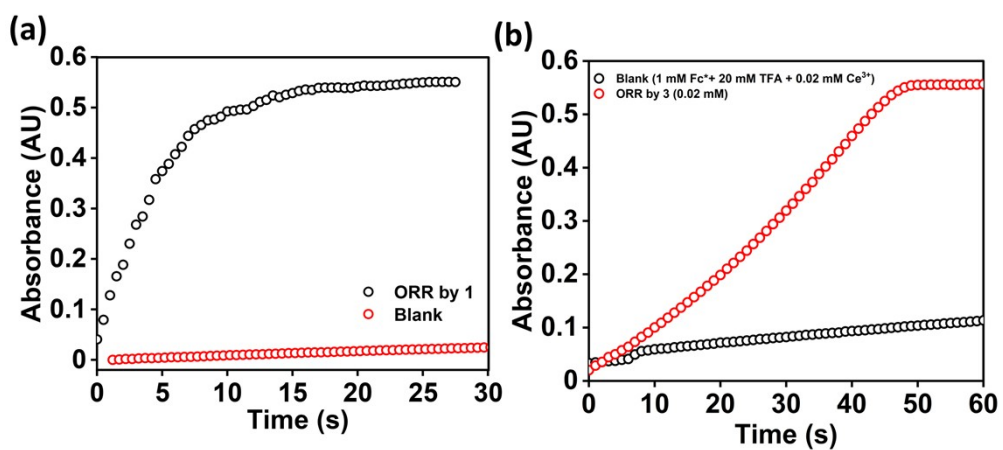


Figure S56. ORR by 1 (a) and 3 (b) and their corresponding blank experiments under a similar reaction condition ($\text{Fc}^* = 1 \text{ mM}$, $\text{TFAH} = 20 \text{ mM}$, $\text{O}_2 = 8.1 \text{ mM}$).

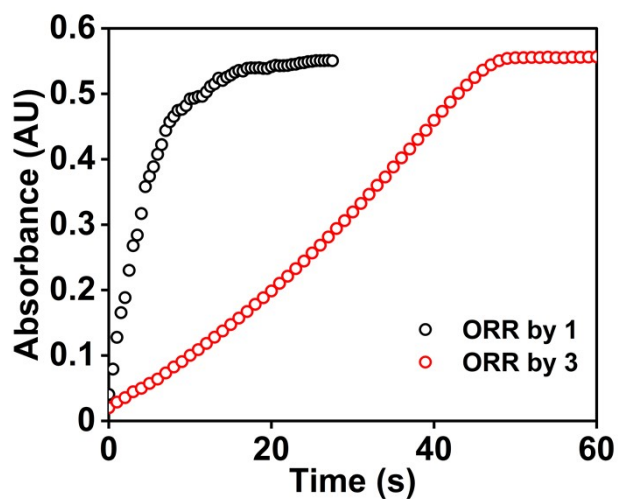


Figure S57. ORR by 1 and 3 under similar conditions. (Complex conc: 0.02 mM , TFAH : 20 mM , Fc^* : 1 mM).

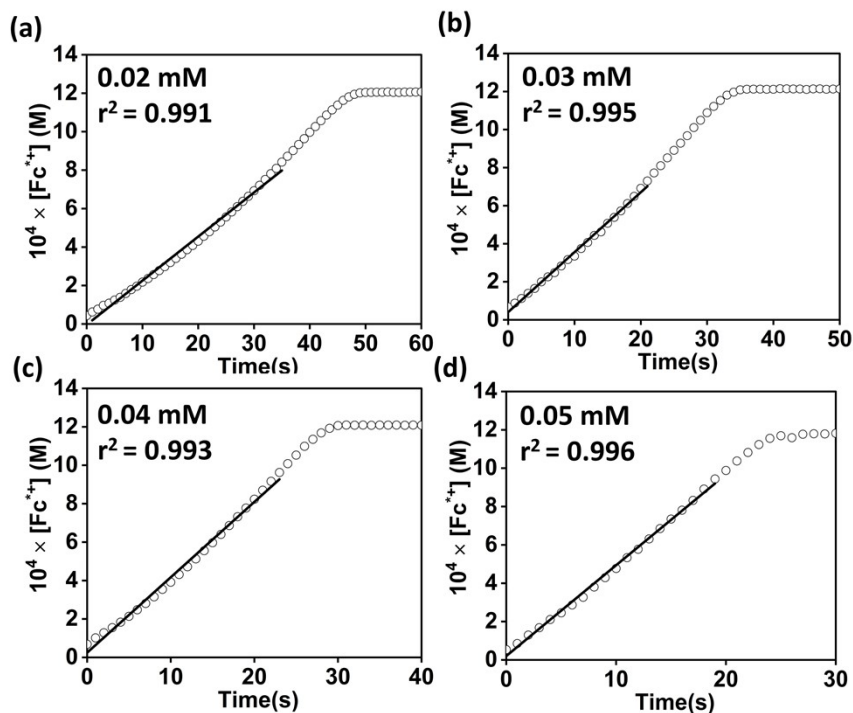


Figure S58. Change of absorbance in the UV-vis spectrum at 780 nm for the reaction of Fc* (1 mM) with O₂ (8.1 mM) in the presence of 20 mM of TFAH and 3 (0.02 mM (a), 0.03 mM (b), 0.04 mM (c), 0.05 mM (d)) at 25 °C.

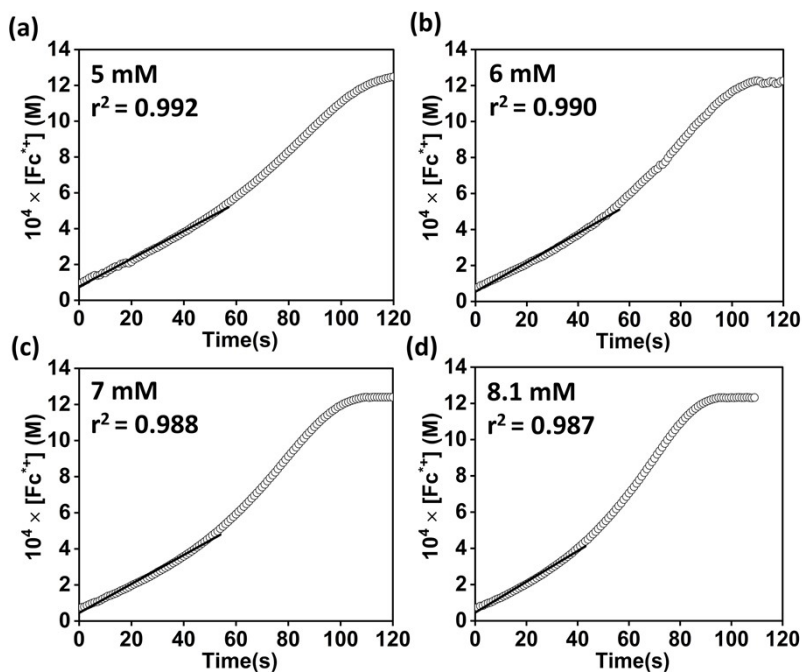


Figure S59. Change of absorbance in the UV-vis spectrum at 780 nm for the reaction of Fc* (1 mM) with O₂ (5.0 mM (a), 6.0 mM (b), 7.0 mM (c), 8.1 mM (d)) in the presence of 20 mM of TFAH and 0.02 mM of 3 at 25 °C.

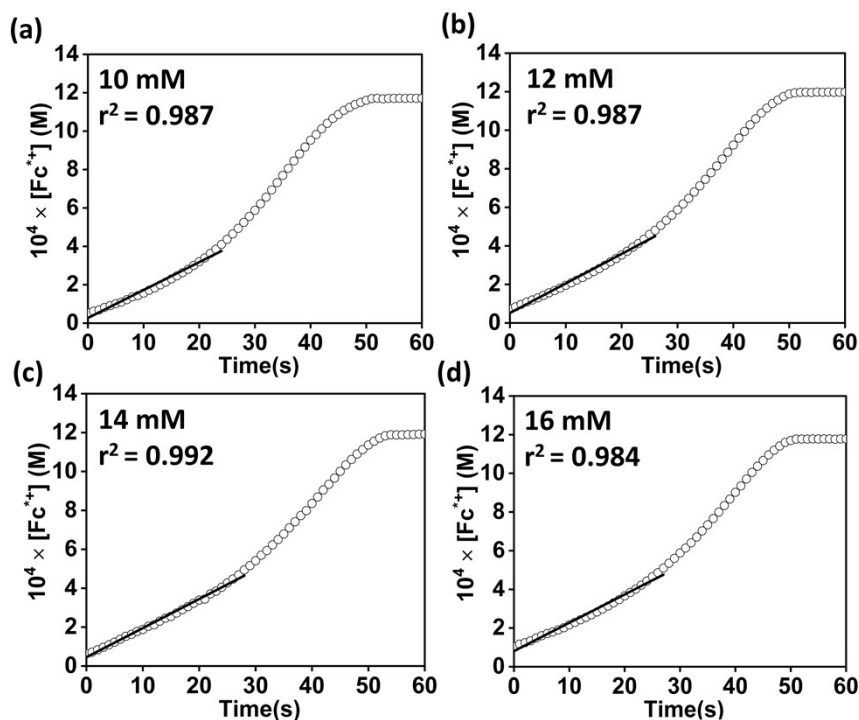


Figure S60. Change of absorbance in the UV-vis spectrum at 780 nm for the reaction of Fc* (1 mM) with O₂ (8.1 mM) in the presence of 0.02 mM of **3** and TFAH (10 mM (a), 12 mM (b), 14 mM (c), 16 mM (d)) at 25 °C.

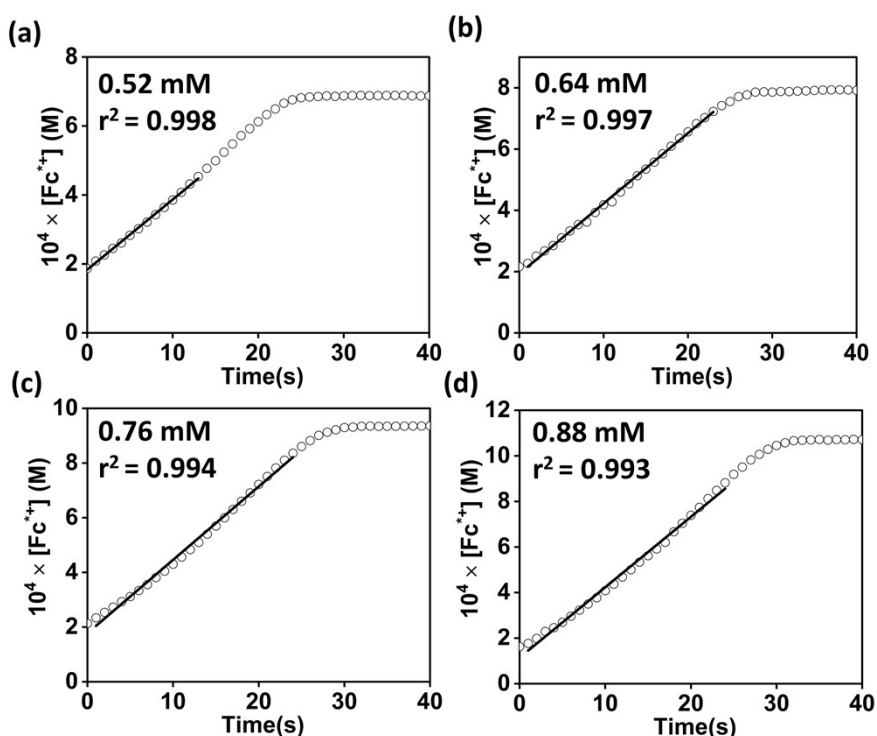


Figure S61. Change of absorbance in the UV-vis spectrum at 780 nm for the reaction of Fc* (0.52 mM (a), 0.64 mM (b), 0.76 mM (c), 0.88 mM (d)) with O₂ (8.1 mM) in the presence of 20 mM of TFAH and 0.02 mM of **3** at 25 °C.

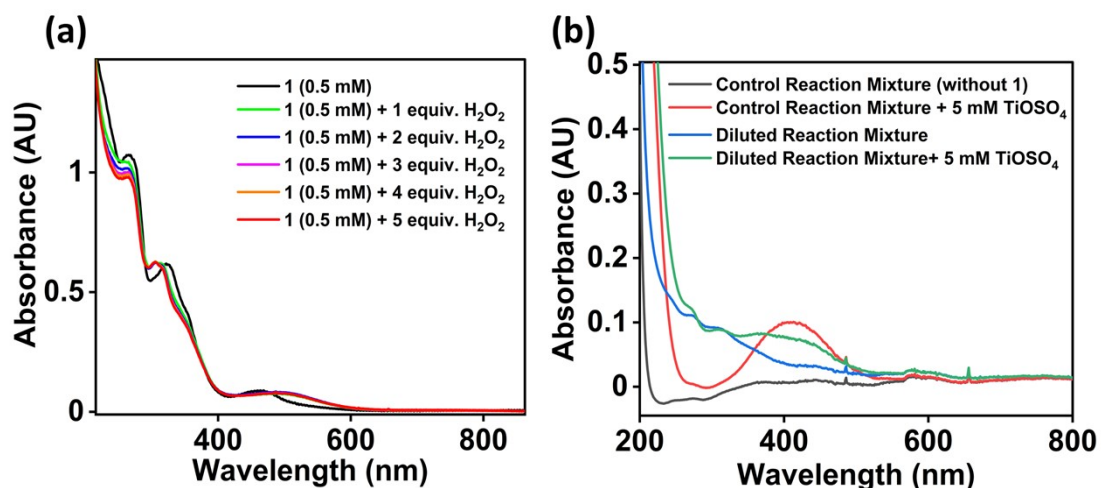


Figure S62. (a) Change of the UV-vis spectrum of **1** (0.5 mM) upon addition of varying equiv. of H₂O₂ at 25 °C. (b) Determination of H₂O₂ by Ti(O)SO₄ assay.

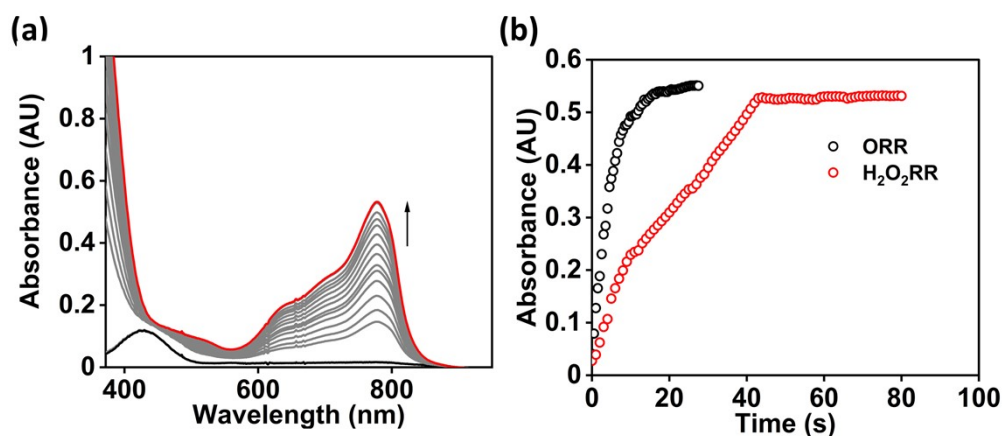


Figure S63. (a) Change of UV-vis spectrum of **1** (0.02 mM) in the presence of Fc* (1 mM), THAH (20 mM), and urea•H₂O₂ (4 mM). (b) Time-dependent formation of Fc*⁺ in the ORR and H₂O₂RR catalyzed by **1** (0.02 mM) at 25 °C in the presence of Fc* (1 mM), TFAH (20 mM), and O₂ (8.1 mM) or urea•H₂O₂ (4 mM).

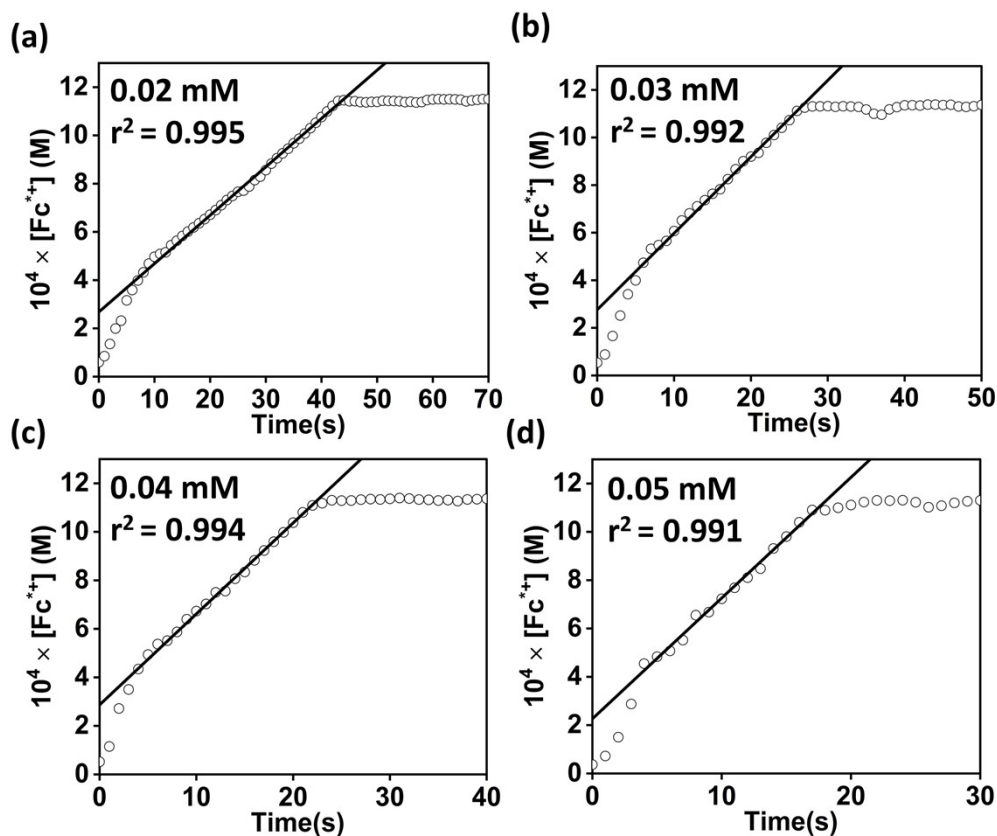


Figure S64. Change of absorbance in the UV-vis spectrum at 780 nm for the reaction of Fc* (1 mM) with urea•H₂O₂ (4 mM) in the presence of 20 mM of TFAH and 1 (0.02 mM (a), 0.03 mM (b), 0.04 mM (c), 0.05 mM (d)) at 25 °C.

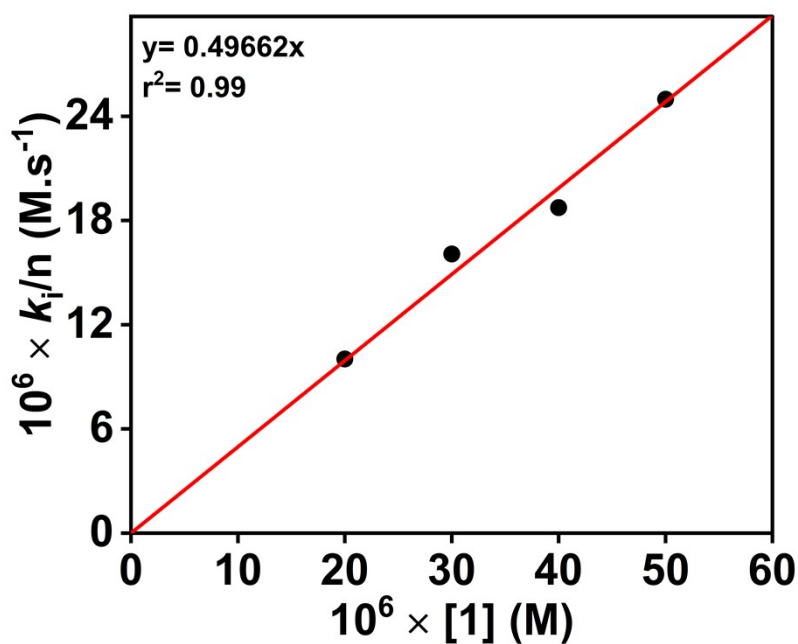


Figure S65. A plot of k_i vs. $[1]$ at a fixed concentration of urea•H₂O₂ (4 mM), TFAH (20 mM), and Fc* (1 mM) at 25 °C.

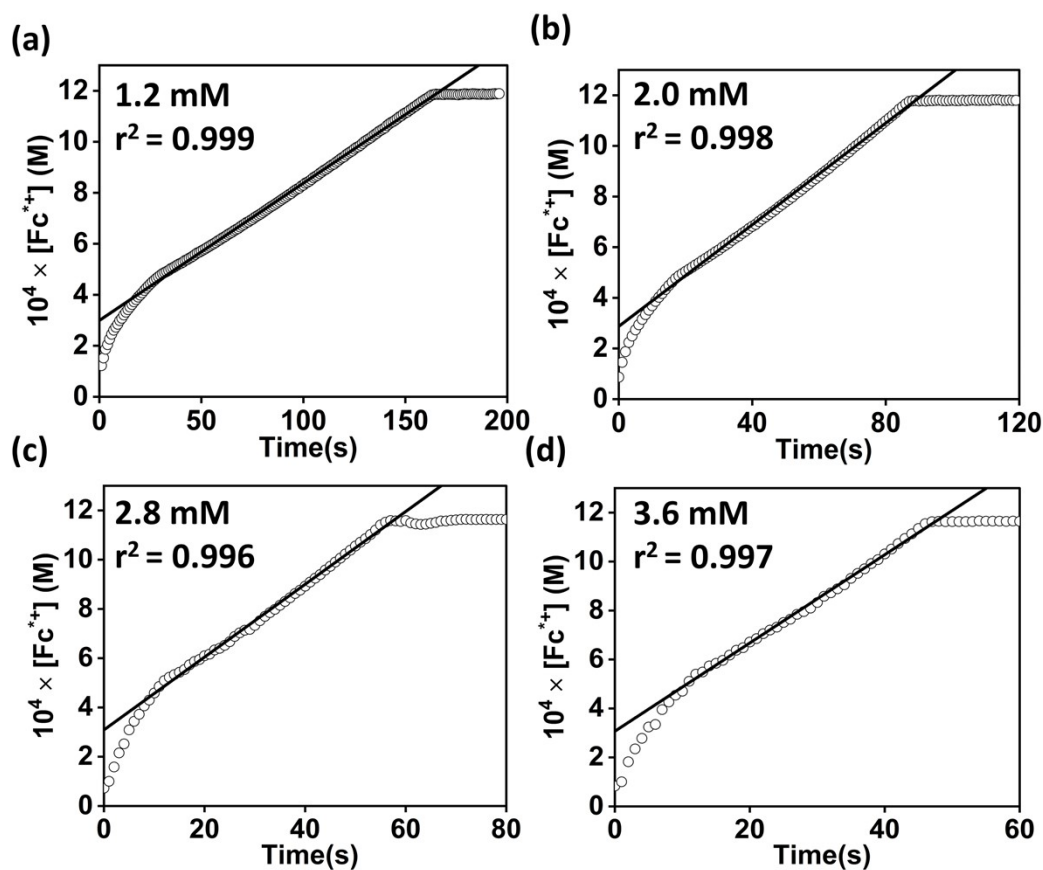


Figure S66. Change of absorbance in the UV-vis spectrum at 780 nm for the reaction of Fc^* (1 mM) with urea• H_2O_2 (1.2 mM (a), 2 mM (b), 2.8 mM (c), 3.6 mM (d)) in the presence of 20 mM of TFAH and 0.02 mM of **1** at 25 °C.

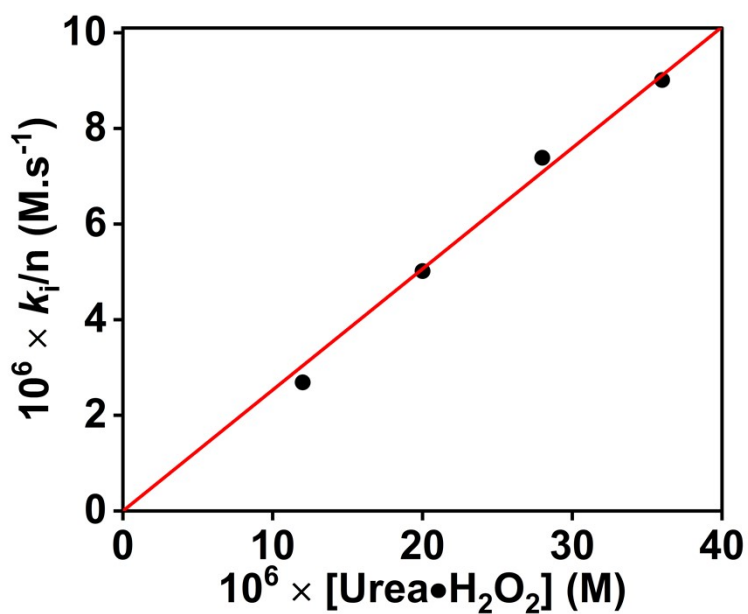


Figure S67. A plot of k_i vs. $[\text{urea}\cdot\text{H}_2\text{O}_2]$ at a fixed concentration of **1** (0.02 mM), TFAH (20 mM), and Fc^* (1 mM) at 25 °C.

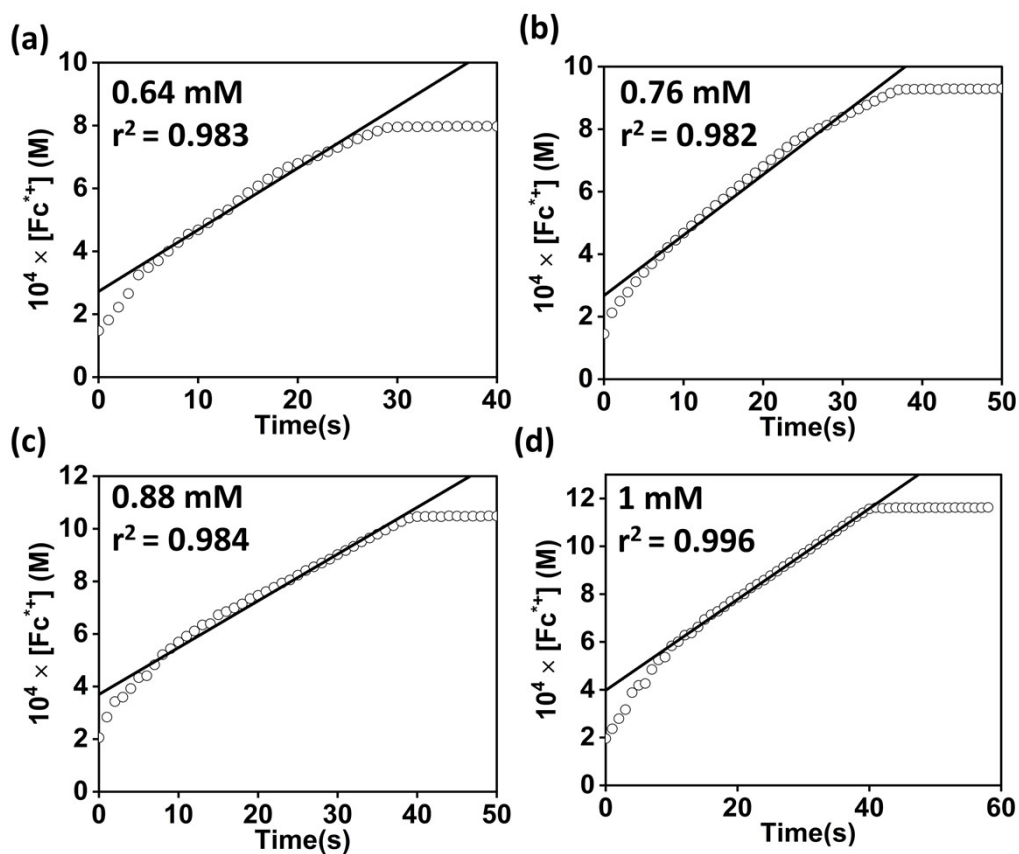


Figure S68. Change of absorbance in the UV-vis spectrum at 780 nm for the reaction of Fc^* (0.64 mM (a), 0.76 mM (b), 0.88 mM (c), 1 mM (d)) with $\text{urea}\cdot\text{H}_2\text{O}_2$ (4 mM) in the presence of 20 mM of TFAH and 0.02 mM of **1** at 25 °C.

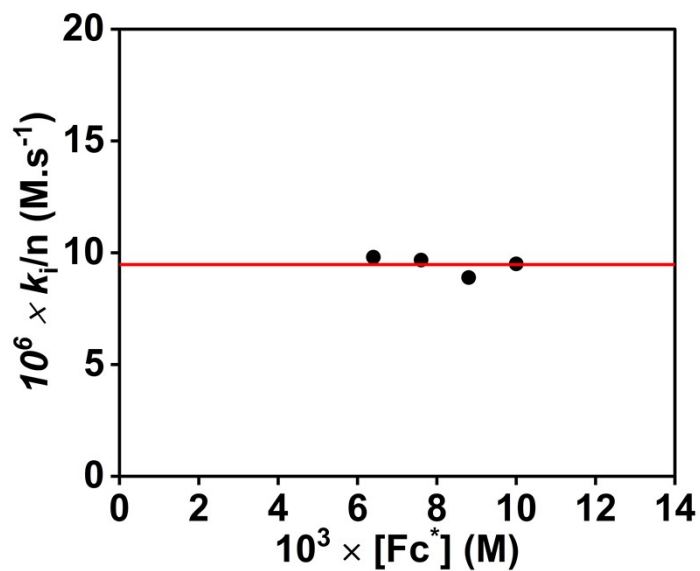


Figure S69. A plot of k_i vs. $[\text{Fc}^*]$ at a fixed concentration of **1** (0.02 mM), $\text{urea}\cdot\text{H}_2\text{O}_2$ (4 mM), and TFAH (20 mM) at 25 °C.

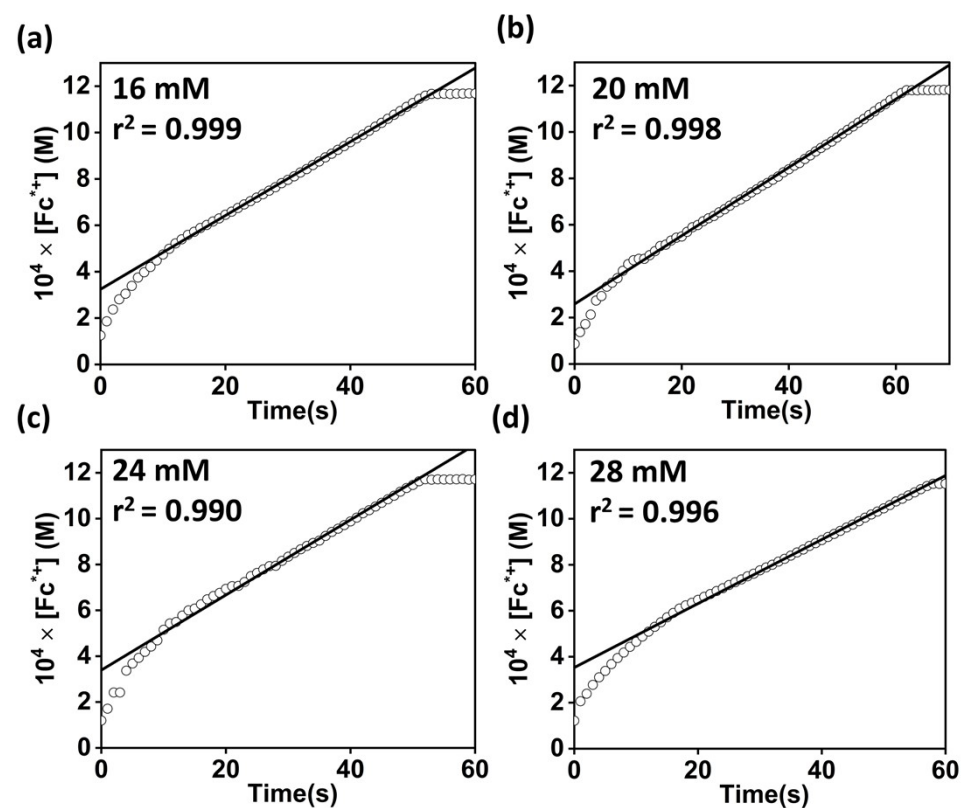


Figure S70. Change of absorbance in the UV-vis spectrum at 780 nm for the reaction of Fc* (1 mM) with urea•H₂O₂ (4 mM) in the presence of 0.02 mM of **2** and TFAH (16 mM (a), 20 mM (b), 24 mM (c), 28 mM (d)) at 25 °C.

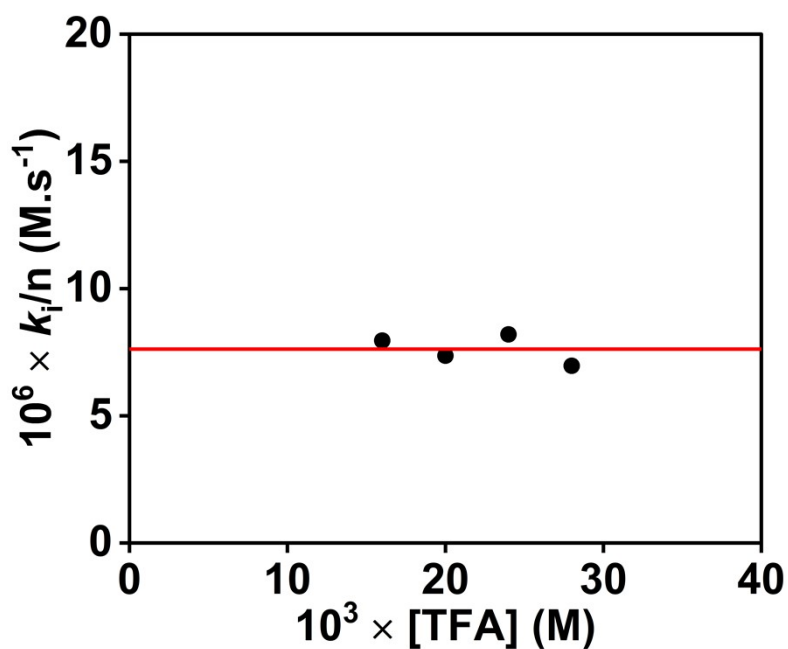


Figure S71. A plot of k_i vs. [TFAH] at a fixed concentration of **1** (0.02 mM), urea•H₂O₂ (4 mM), and Fc* (1 mM) at 25 °C.

References

- 1 W. C. Wolsey, *J. Chem. Educ.*, 1973, **50**, A335-A337.
- 2 E. N. Cook, D. A. Dickie and C. W. Machan, *J. Am. Chem. Soc.*, 2021, **143**, 16411–16418.
- 3 M. L. Pegis, C. F. Wise, D. J. Martin and J. M. Mayer, *Chem. Rev. (Washington, DC, U. S.)*, 2018, **118**, 2340-2391.
- 4 B. D. McCarthy, D. J. Martin, E. S. Rountree, A. C. Ullman and J. L. Dempsey, *Inorg. Chem.*, 2014, **53**, 8350-8361.
- 5 A. J. Sathrum and C. P. Kubiak, *J. Phys. Chem. Lett.*, 2011, **2**, 2372-2379.
- 6 J. M. Saveant and E. Vianello, *Electrochim. Acta*, 1963, **8**, 905-923.
- 7 A. J. Bard and L. R. Faulkner, *Electrochemical Methods: fundamentals and applications*, John Wiley & Sons, Inc., New York, 2001.
- 8 G. M. Sheldrick, *Acta Crystallogr., Sect. A Found. Crystallogr.*, 2008, **A64**, 112-122.
- 9 C. F. Macrae, I. J. Bruno, J. A. Chisholm, P. R. Edgington, P. McCabe, E. Pidcock, L. Rodriguez-Monge, R. Taylor, J. van de Streek and P. A. Wood, *J. Appl. Crystallogr.*, 2008, **41**, 466-470.
- 10 A. Das, A. Ali, G. Gupta, A. Santra, P. Jain, P. P. Ingole, S. Paul and S. Paria, *ACS Catal.*, 2023, **13**, 5285-5297.